POLITECNICO DI MILANO

SCHOOL OF INDUSTRIAL AND INFORMATION ENGINEERING

MASTER OF SCIENCE IN MATHEMATICAL ENGINEERING

INGEGNERIA MATEMATICA

MODELLING AND SIMULATION OF NEAR-WELLBORE FORMATION DAMAGE AND INHIBITION PROCESS

Supervisor: Prof. Giovanni Michele Porta
Co-Supervisor: Dott. Iacopo Borsi

Master Thesis by:
Ayisha Mahmudova 878164

Academic Year 2019/2020

Acknowledgements

I would first like to thank to my thesis supervisor Prof. Giovanni Michele Porta from the Department of Civil and Environmental Engineering at Politecnico di Milano. Without his contributions and advices this thesis could not have been successfully conducted.

I am very grateful to my co-supervisor Dott. Iacopo Borsi at TEA Sistemi for his patience, motivation and guidance. His door was always open whenever I ran into trouble or had a question about my research.

I would like to thank also CHIMEC S.p.A. for their assistance with collecting the laboratory and field data.

I would also like to acknowledge my colleague Andrea Fani from TEA Sistemi who was always happy to lend a hand to build my model.

My sincere gratitude also goes to my colleague and friend Cristiano di Benga for helping me to have the opportunity to do internship in TEA Sistemi.

I must express my very profound gratitude to my parents for providing me with unfailing support throughout years of my study. This accomplishment would not have been possible without them.

Finally, I feel immensely grateful to my beloved Roberto Pasciuti, for always standing by me with his endless support and continuous encouragement.

Ayisha Mahmudova

May 2020

Abstract

The phenomenon of permeability reduction in the zone near a well (called *formation damage* or *scaling*) is a well-known problem in oil & gas and geothermal energy industry. Precipitation of dissolved species (such as calcite, dolomite, asphaltene, paraffin, etc.) can result in formation damage and failure in production during processing of the reservoir. Damage in the subsurface formation caused by organic and inorganic precipitation decreases the porosity and permeability, eventually reducing the production rate. When the flow pathways and pore spaces are plugged, fluid flow decreases substantially resulting in loss of efficiency in the reservoir exploitation. Quite frequently larger pumps need to be installed or the operation period is extended to meet demand.

A possible solution to this problem consists in stopping the production followed by the injection of inhibiting species that slow down the precipitation process. Inhibitor injection is widely used and is an effective method to prevent the precipitation which provides a reliable long-term protection against formation scaling.

In this thesis, the focus is given to the mineral precipitation. A mathematical model is built to express the precipitation and the corresponding inhibition process, starting from classical model formulations proposed in the literature. Sensitivity analysis is performed with various values for saturation index of precipitating mineral and inhibitor properties to test the efficiency of the inhibiting species. The efficiency is determined by adsorption and desorption properties of the inhibitor, and its concentration in the injection fluid.

Two scenarios, namely, normal production and production with inhibitors are compared. As the key output the pressure in the well-bottom is monitored. Well-bottom pressure decreases as a result of permeability damage by the precipitation, and from the simulation it is obtained that during the production with the inhibitor this decrease is slower with respect to the normal production, which allows longer exploitation of the reservoir.

The objectives of this work were suggested by the company TEA SISTEMI S.p.A., which hosted the thesis internship. Laboratory and field data are shared with the Author by CHIMEC S.p.A., a partner of TEA SISTEMI, a company designing and producing additive for the oil & gas sector.

Sintesi

Il fenomeno della riduzione di permeabilità del mezzo poroso nella zona circostante un pozzo (noto come formation damage o scaling) è un problema ben noto nel campo dell'industria petrolifera, del gas e della produzione di energia geotermica. La precipitazione di specie disciolte dà luogo alla formazione di materiali solidi (come calcite, dolomite, asfaltene, paraffina, ecc.) e può provocare danni al giacimento e inconvenienti nel processo di produzione. I danni causati da precipitazioni organiche e inorganiche diminuiscono la porosità e la permeabilità, riducendo così il tasso di produzione. Quando il volume disponibile all'interno del mezzo poroso viene ridotto, il flusso di fluido diminuisce sostanzialmente con conseguente perdita di efficienza di sfruttamento del giacimento. In tal caso, è piuttosto frequente la necessità di installare pompe più potenti o di allungare i tempi di estrazione.

Una possibile soluzione a questo problema consiste nell'arresto della produzione seguita dall'iniezione di sostanze inibitrici che rallentano il processo di precipitazione. L'iniezione dell'inibitore è un metodo ampiamente utilizzato ed efficace per prevenire la formazione di precipitati solidi, ed esso fornisce una protezione affidabile a lungo termine contro il ridimensionamento della formazione.

In questa tesi, l'attenzione è rivolta alla precipitazione di minerali. A partire dalle formulazioni matematiche classiche documentate in letteratura, è stato sviluppato un modello matematico con l'obiettivo di descrivere sia il processo di precipitazione e che il corrispondente processo di inibizione. Per verificare l'efficacia di differenti specie inibenti, è stata eseguita un'analisi di sensitività basata sia sui valori degli indici di saturazione, calcolati tramite simulazione numerica della precipitazione dei minerali, sia sulla variazione delle proprietà delle specie inibenti. Il grado di efficienza del trattamento è determinato dalle proprietà di adsorbimento e desorbimento dell'inibitore e dalla sua concentrazione nel fluido di iniezione.

Nelle simulazioni vengono confrontati due schemi produttivi, vale a dire la normale produzione senza utilizzo di inibitori e la produzione con inibitori. L'indicatore utilizzato per determinare l'efficienza del processo è stata la pressione sul fondo del pozzo: la pressione infatti diminuisce in seguito alla riduzione di permeabilità causata dalle precipitazioni. Le simulazioni evidenziano che, durante la produzione con l'inibitore, questa diminuzione risulta più lenta rispetto alla produzione normale, risultato che consente uno sfruttamento più proficuo del giacimento.

Gli obiettivi di questo lavoro sono stati proposti dalla società TEA SISTEMI S.p.A., azienda nella quale è stato svolto il tirocinio di tesi. I dati di laboratorio e di campo sono invece stati condivisi con l'autrice da CHIMEC S.p.A., azienda partner di TEA SISTEMI, impegnata nella progettazione e produzione di additivi per il settore petrolifero e del gas.

Contents

INTRODUCTION **1**
Chapter 1: PROBLEM SETTING AND MOTIVATION **5**
1.1 Flow and Transport Processes in Porous Media 5
1.1.1 Properties of porous media 5
1.1.2 Darcy's law and its validity range 7
1.1.3 Types of transport in porous media 9
1.1.4 Adsorption and desorption 11
1.2 Mineral Precipitation and Inhibition Treatment 12
1.2.1 Types of precipitation 12
1.2.2 Causes of precipitation 13
1.2.3 Reservoir remediation techniques 15
Chapter 2: MATHEMATICAL MODEL **17**
2.1 Model Definition and Assumptions 17
2.2 System of PDEs and Constitutive Laws 19
2.3 Initial and Boundary Conditions 25
2.4 Dimensionless Equations 26
2.5 More on the Pressure Equation 27
Chapter 3: NUMERICAL MODEL **31**
3.1 Numerical Methods for the Equations 31
3.2 Stability Analysis of the Explicit Euler Method 37
3.3 Convergence Criteria 38
3.4 Solution Set-up 40
Chapter 4: NUMERICAL RESULTS AND ANALYSIS **47**
4.1 Reference Case 47
4.2 Code verification 55
4.3 Sensitivity analysis 59
Chapter 5: CONCLUSIONS AND FUTURE DEVELOPMENTS **63**
APPENDIX **67**
References **69**

List of notations

p	pressure, [Pa]
u	Darcy's flux, [m/s]
$\mathbf{v}$	average velocity field, [m/s]
k	absolute average horizontal permeability, [m^2]
ϕ_0	effective initial porosity, [-]
ϕ	effective porosity, [-]
β	fluid compressibility, [Pa^{-1}]
ρ	fluid density, [kg/m^3]
μ	dynamic fluid viscosity, [Pa s]
D_{diff}	molecular diffusion, [m^2/s]
D_{disp}	mechanical dispersion, [m^2/s]
a_L	dispersivity, [m]
c_p	precipitation concentration, [$mole/m^3$]
R_p	precipitation rate, [$mole/m^3/s$]
R_{pi}	precipitation rate after injecting the inhibitor, [$mole/m^3/s$]
k_p	reaction constant, [$mole/m^2/s$]
S	specific surface area of the pore space, [m^3/m^2]
Λ	saturation index of calcite, [-]
m	precipitation rate exponent, [-]
V_s	molar volume of calcite, [$m^3/mole$]
ρ_b	bulk density of the porous media, [kg/m^3]
c_i	inhibitor concentration, [kg/m^3]
F	mass of the adsorbed inhibitor per unit mass of the solid, [-]
F_{max}	maximum inhibitor adsorption fraction, [-]
b	inhibitor adsorption energy coefficient, [m^3/kg]
η	inhibitor efficiency coefficient, [-]
n	inhibitor efficiency exponent, [-]
ε_p	fractional bulk volume, [-]

INTRODUCTION

Formation damage is a generic terminology referring to the impairment of the permeability of subsurface reservoirs by various adverse processes [1]. It is a common problem in the production wells that produce oil, gas or geothermal fluids. Being an almost irreversible process, if not treated on time and properly, formation damage prevents the efficient exploitation of reservoirs. Diagnosis and monitoring of the formation damage performed by well testing, well logging, reservoir history matching and the analysis of the produced fluid can be used to obtain information about the possible damage in the future [1]. Many different reasons of formation damage include mechanical deformation under stress and fluid shear, fracturing due to the drilling processes, clay and shale swelling [1]. We focus in this work on the impact of the precipitation of dissolved substances in the formation fluid. The figure below shows flow pathways being blocked/reduced as a result of precipitation.

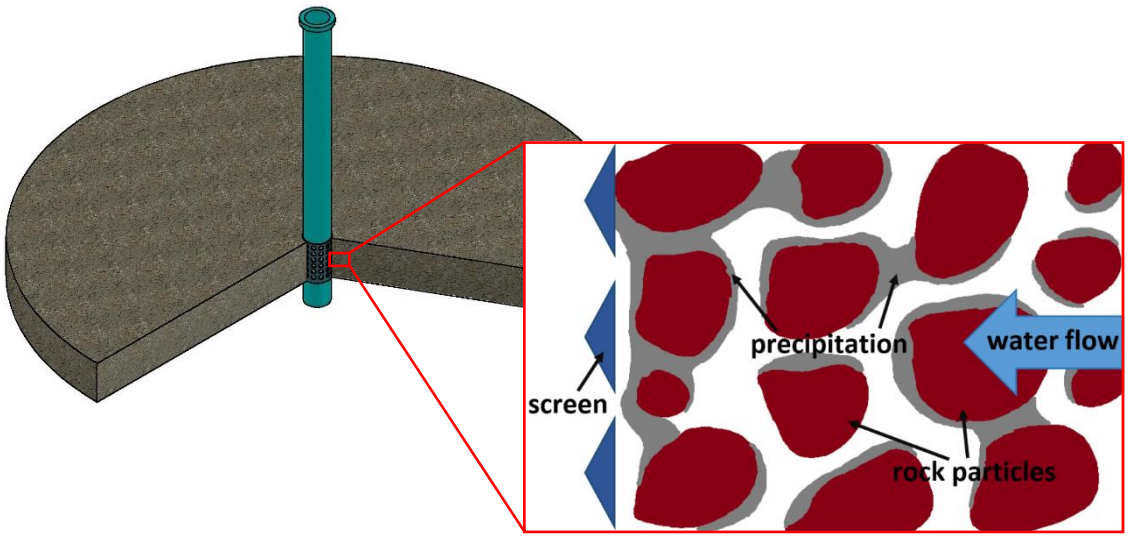

To prevent the precipitation, inhibitors are used during fracturing, shut-in and flowback stages. Inhibitors have been used successfully to control scale formation in conventional oil, gas and geothermal water production. The most widely used technique to deliver the scale inhibitors to the formation system is an injection treatment, during which inhibitors are pumped into the formation and retained in the reservoir [1]. When production resumes, inhibitors flow back with the produced fluid and adsorb on the rock surface, giving protection against scaling. The reactions between inhibitors and formation minerals determine the inhibitor retention and release after inhibitor injection treatment.

It is known from the literature that the inhibitor must have some affinity with the host rock to be adsorbed on its surface and modify the kinetics of mineral precipitation dissolution. However, the precise mechanism by which the inhibitor affects this process

is not understood clearly. The action of precipitation inhibitors is based on the adsorption processes of the inhibitor itself on the solid matrix.

In this thesis the goal is to develop a mathematical model for mineral precipitation and the inhibition treatment by injection.

The complete mathematical model is based on models already available in literature and is established as a system of partially differential equations and constitutive laws that express several dynamics involved. Within this thesis work a numerical code is implemented and simulates 2 scenarios of the process, namely:

a) *Normal production*. Extraction of reservoir fluid and precipitation of species which induces a reduction in the porosity and permeability of the medium.

b) *Production with inhibitor*. It is composed of two phases (cycles) which are performed periodically:

    1) *Injection* of inhibitor from the same well for a predetermined amount of time.

    2) *Production* while the inhibitor is present in the reservoir.

Simulation is performed for various schemes by changing the saturation index and the precipitation rate of the dissolved species, and the inhibitor properties (concentration, injection time and adsorption rate).

Output of the simulations is the set of unknown variables like pressure, permeability, fluid velocity and solute concentrations. Numerical simulations allow obtaining an approximation of these variables during the two processes (namely, normal production and production with inhibitor) and increasing our understanding of the involved processes. As a result, this may help in increasing the efficiency of the inhibitor application.

In general, the efficiency of the inhibitor treatment is analysed by experiments in a laboratory creating the well-bottom environment and the effect of the inhibitor has never been quantitatively observed. This thesis aims to build a mathematical model based on PDE for a computer simulation. In this thesis we:

- provide a simplified model around a production well on a one-dimensional radial domain;
- build a computer code to perform numerical simulation of the model based on finite difference method;
- estimate the exploitation time of a production well during the normal production, having given the concentration of the precipitating substance and the precipitation rate (which depends on e.g. temperature) at the well-bottom;
- build a model to describe the effect of the inhibitor on the precipitation rate of the precipitating substance;
- estimate the exploitation time of the same production well during the production with inhibitor with the given inhibitor concentration and injection time;

- compare the two scenarios, namely, normal production and the production with inhibitor, to understand the effectiveness of the inhibitor injection treatment.

This document is organized as follows: Chapter 1 introduces porous media properties and transport processes along with a brief survey of chemical precipitation types and sources, and industrially used treatment techniques. Complete mathematical and numerical model formulations and implementation details are contained in Chapter 2 and 3, respectively. In Chapter 4 we analyze the output of the simulations for the reference scenario, and perform a code verification and sensitivity analysis. Finally, Chapter 5 includes the conclusions and further development envisaged in future activities.

This project has been developed in TEA Sistemi SpA (TEA) which is a private Italian company that provides research, development and consultancy services in energy and environment sector. The company activities cover the fields of environmental engineering, health safety and environmental risk analysis, subsea, topside and down-hole processing and separation. TEA also supports internal R&D activities and develops proprietary know-how which now represents a consistent asset of the Company.

Chapter 1: PROBLEM SETTING AND MOTIVATION

1.1 Flow and Transport Processes in Porous Media

Flow in porous media is a great interest to many fields of engineering. The aim of this section is to give the fundamental background about reservoirs and transport in porous media. Starting from the properties of porous media we will present the well-known Darcy's law, types of transport and typical processes, such as adsorption and desorption happening in porous media.

1.1.1 Properties of porous media

A reservoir is a geological formation that contains fluids (oil, gas, fresh and saline water, geothermal fluids) in its pore space. As will be shown in the next sections, our approach is to model a system of partial differential equations (PDE) and these equations are based on the assumption that the porous medium is described as continuum; therefore, the models we employed are referred to as continuum models.

The portion of the rock which is occupied by the fluid is called pore space and the solid phase is known as solid matrix. General properties of porous media to transmit and store the fluids are defined numerically through a number of parameters. Referring to the porous medium as continuum, a short description of the main porous media properties that are used in this thesis is given in the following.

Porosity. Porosity, ϕ [-], is defined as the volume of the pores of a soil sample, U_p [m^3], divided by the total volume, U_t [m^3], of both pores and solid matrix.

$$\phi = \frac{U_p}{U_t} \tag{1.1.1}$$

There exist two types of porosity in a rock: *primary porosity* is formed at the time of the deposition of the soil, *secondary porosity* is induced by fracturing, deformation, dissolution and precipitation. The total porosity is the sum of primary and secondary porosities [2].

A crucial feature of porous media is connectivity. A rock can be thought as a solid matrix pores, but to allow flow and transport of matter these pores have to be interconnected, so that the fluid can flow through continuous paths. In general, there can be also unconnected and dead-end pores. The interconnected pore space is defined as the

effective porosity, ϕ_e [-], and it is the parameter used mostly in the applications [3] (later on the index in ϕ_e is dropped for simplicity). Porosity is defined as a volume ration and can be equivalently indicated as a percentage [2].

Absolute permeability. Being one of the most fundamental property of a porous medium absolute permeability (or intrinsic permeability), k [m^2], is the measure of ability to transmit the fluids through the soil. It is a property of the medium and has nothing to do with the temperature, pressure or the fluid flowing through the medium. Permeability can be defined as [4]

$$k = Cd^2 \tag{1.1.2}$$

where d [m] is the average pore size and C [-] is an empirical constant that depends on many factors, such as packing, sorting, etc.

The standard measurement unit of permeability is [m^2], but the practical unit of permeability is called darcy (D), named after Henry Darcy:

$$1\ D \approx 10^{-12}\ m^2 \tag{1.1.3}$$

Fig. 1.1.1 shows the permeability range for some rocks [5]. Notice that the permeability is really unconstrained – even for one rock type it may span several orders of magnitude.

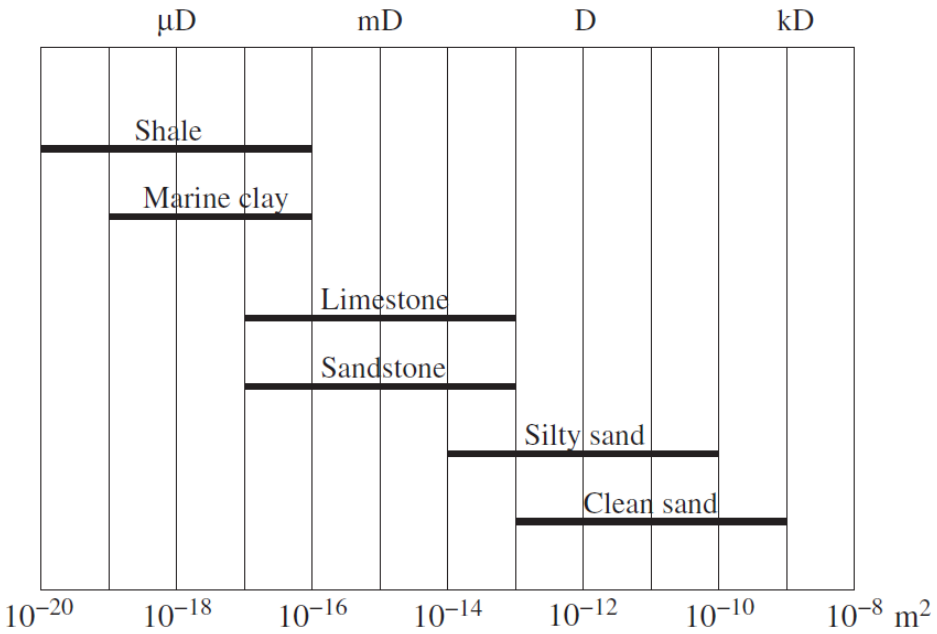

Figure 1.1.1: Permeability of common sedimentary rocks (ref: [5])

When k varies in space we refer to the porous medium as being inhomogeneous or heterogeneous. If it varies also with direction, the medium is called anisotropic. In this case, the permeability is represented as a second rank tensor.

Hydraulic conductivity. Hydraulic conductivity, K [m/s], for a saturated medium is defined as [4]:

$$K = \frac{k\rho g}{\mu} \tag{1.1.4}$$

where ρ [kg/m^3] is the fluid density, μ [kg/m/s] is dynamic viscosity of the fluid and g [m/s^2] is the gravitational acceleration. Since it depends on the permeability of the rock and on the viscosity of the fluid, it is a property of the whole medium, including the porous matrix and the fluid hosted in the pore space.

Hydraulic head. Hydraulic head at a point in a reservoir is defined as

$$h = z + \frac{p}{\rho g} \tag{1.1.5}$$

where z [m] is the distance to the reference point (usually sea level), p [kg/m/s^2] is the fluid pressure measured at that point. Fluid potential and hydraulic head are equivalent notions, and both are used in applications.

1.1.2 Darcy's law and its validity range

Forming the basis of hydrogeology, Darcy's law is nothing but the momentum balance equation for the fluids flowing in a porous medium.

Darcy derived his law from experiment on a column filled with sand and water. The law can easily be extended to the case of one-dimensional flow in the inclined column of saturated, homogeneous porous medium shown in Fig. 1.1.2 [4]. Darcy's law states that the flow rate through the column, Q [m^3/s], is proportional to the cross-sectional area, A [m^2], and to the difference between the hydraulic heads, $h_1 - h_2$ [m], and inversely proportional to length of the column, L [m], and reads as [4]

$$Q = KA\left(\frac{h_1 - h_2}{L}\right) \tag{1.1.6}$$

where the coefficient of proportionality, K, is the hydraulic conductivity. Substituting the definitions of the hydraulic head (1.1.5) and hydraulic conductivity (1.1.4) from the previous section and defining the specific discharge, $u = {}^{Q}/_{A}$ [m/s], (which later will be called Darcy's flux) we obtain

$$u = \frac{k}{\mu}\left(\frac{p_1 - p_2}{L} + \rho g\frac{z_1 - z_2}{L}\right), \quad \rho g = \gamma \tag{1.1.7}$$

where γ [kg/m/s^2] is the specific weight of the fluid.

When the flow is three-dimensional this law takes the form as

$$\mathbf{u} = \frac{\mathbf{k}}{\mu}(\nabla p + \rho g \nabla z) \tag{1.1.8}$$

where **k** is the second rank permeability tensor. Permeability is in tensor form, since the pressure can be applied in three directions, and measured for each direction leads to a 3 by 3 tensor. The tensor is often written in a matrix form and is both symmetric and positive definite, in cartesian coordinates reads as [3]

$$\mathbf{k} = \begin{bmatrix} k_{xx} & k_{xy} & k_{xz} \\ k_{yx} & k_{yy} & k_{yz} \\ k_{zx} & k_{zy} & k_{zz} \end{bmatrix} \tag{1.1.9}$$

Because of the symmetry there are only 6 different components ($k_{ij} = k_{ji}$). When the porous medium is homogeneous, permeability tensor reduces to a diagonal tensor, and if also isotropic, then the diagonal components are all equal.

Validity range of Darcy's law. Experiments showed that when the specific discharge increases, the linear relationship between the specific discharge and the hydraulic gradient appears to be invalid [4]. Therefore, it is necessary to define the applicability range of this law. To do this, the well-known Reynolds number Re, a dimensionless quantity, which is the ratio between inertial and viscous forces, is used:

$$Re = u\frac{d}{\nu} \tag{1.1.10}$$

where d [m] is the length representing the dimensions of the pore space and $\nu = {}^{\mu}/_{\rho}$ [m^2/s] is the kinematic viscosity [4]. Experiments show that deviations from Darcy's law start at $Re \cong 5$ and when Re is around 60 turbulent flow occurs [2]. Moreover, in rocks with large fractures or karstic limestones, because of large d Darcy's law is not valid [2].

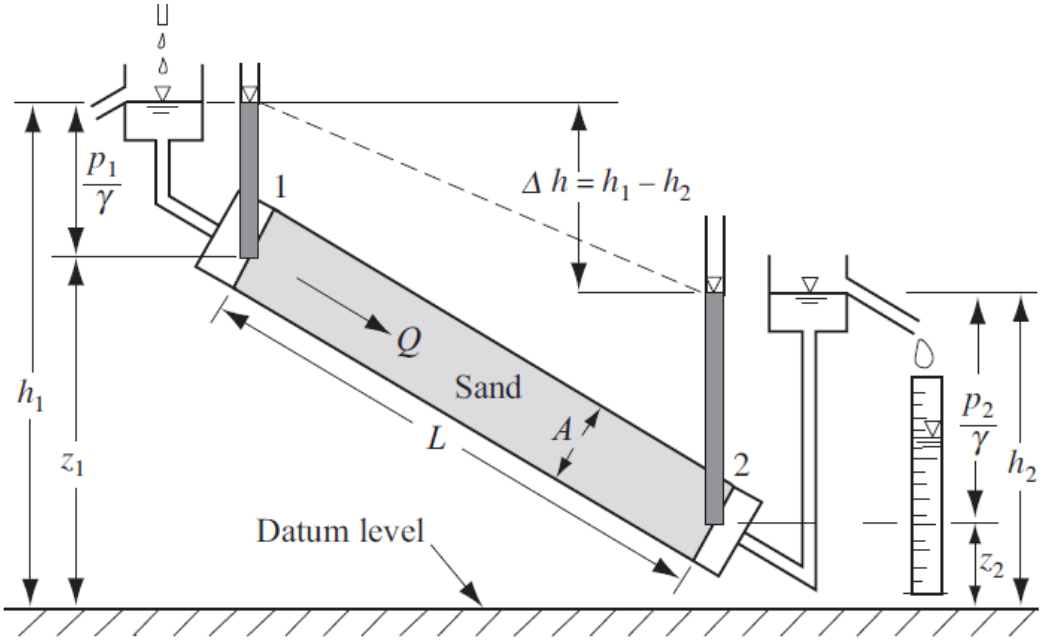

Figure 1.1.2: Seepage through an inclined sand filter (ref: [4])

1.1.3 Types of transport in porous media

Transport of dissolved species in porous media is an important subject in order to understand the movement of chemicals, such as contaminants, minerals, inhibitors, that are dissolved in the void space of a porous medium domain. The fundamental transport mechanisms that occur in a saturated porous medium are presented below [4] [2]:

Advection. Advection governs the motion of a scalar field (in our case, concentration of a substance) under the action of a known velocity vector field. The advective flux, $\mathbf{J}_{adv}$ [mole/m^2/s], of a considered component is given by [4]

$$\mathbf{J}_{adv} = \mathbf{v}\, c \tag{1.1.11}$$

where $\mathbf{v}$ [m/s] is the average velocity of the fluid obtained by dividing the Darcy's flux by the effective porosity:

$$\mathbf{v} = \frac{\mathbf{u}}{\phi_e} \tag{1.1.12}$$

and c [mol/m^3] is the concentration of the dissolved substance.

Diffusion. Effective diffusion in a porous medium is proportional to the molecular diffusion of the fluid but is affected by the presence of solid boundaries. Molecular diffusion is a consequence of random motion that results in random collisions of molecules. The outcome is the spreading of material through these collisions. Fick's first

law related the diffusive flux to the concentration under the steady state assumption. It states that the flux goes from high concentration regions to the law concentration regions. This movement of solute is then proportional to the concentration gradient. Mathematically representing the effective diffusion flux $\mathbf{J}_{diff}$ [mole/m^2/s] is proportional to the gradient of concentration c by the effective diffusion tensor $\mathbf{D}_{diff}$ [m^2/s] (which depends on various factors such as molecule size, density, temperature, porosity, tortuosity, etc.) [2]:

$$\mathbf{J}_{diff} = -\mathbf{D}_{diff} \nabla \mathrm{c} \qquad 1.1.13$$

Normally, molecular diffusion per se is just a coefficient D_{diff}, and $\mathbf{D}_{diff}$ is a second rank symmetric tensor which is defined as [4]:

$$\mathbf{D}_{diff} = D_{diff}\mathbf{T}$$

where $\mathbf{T}$ is the tortuosity tensor that depends on the porosity, $\mathbf{T} = \mathbf{T}(\phi)$. Molecular diffusion is also affected by the fact that viscosity of the fluid is higher near the solid surface than that inside the fluid phase, and viscosity is highly dependent on the temperature.

The negative sign on the right-side of the eq. (1.1.13) means that the flux is in the direction from high to low concentrations.

Dispersion. Differently from diffusion dispersion arises only within a porous medium. In the modeling of transport phenomena dispersion and diffusion are commonly lumped in a single coefficient. However, their physical explanation is completely different, mechanical dispersion is spreading due to pore to pore variation in average velocity while diffusion provides the mixing between chemicals under the effect of concentration gradients. In fact, the term mechanical is used to remind us that the spreading is due to fluid mechanics phenomena. Fick's law can be applied to describe also the dispersive flux $\mathbf{J}_{disp}$ [mole/m^2/s] [2]:

$$\mathbf{J}_{disp} = -\mathbf{D}_{disp} \nabla \mathrm{c} \qquad 1.1.14$$

where $\mathbf{D}_{disp}$ [m^2/s] is the mechanical dispersion second rank tensor that depends on the dispersivity $\mathbf{a}$ [m] of the porous medium which is a fourth rank tensor and the average pore velocity $\mathbf{v}$ [m/s]. For an isotropic medium $\mathbf{a}$ is determined with two components, namely, a_L and a_T which are the *longitudinal* and *transverse dispersivities* of the porous medium, respectively. Then, the components of the dispersion tensor D_{ij} can be expressed in cartesian coordinates with the average velocity field, $\mathbf{v} = [v_x, v_y, v_z]$, as in [4]:

$$D_{ij} = \left[a_T \delta_{ij} + (a_L - a_T)\frac{v_i v_j}{|\mathbf{v}|^2}\right]|\mathbf{v}| \qquad 1.1.15$$

where δ_{ij} is the Kronecker delta.

The sum of molecular diffusion and the mechanical dispersion is called *hydrodynamic dispersion*: [4]:

$$\mathbf{D} = \mathbf{D}_{diff} + \mathbf{D}_{disp} \qquad 1.1.16$$

1.1.4 Adsorption and desorption

Adsorption and desorption refer to the exchange of molecules and ions between the solid phase surface and the liquid phase [2].

Adsorption is the accumulation of molecules and ions present in the liquid phase on the rock material. The solid on which the dissolved species are accumulated is called *adsorbent* and the adsorbing matter is *adsorbate*. Adsorption results in the decrease of the concentration of the dissolved component and causes retardation of the transport. Generally, adsorption does not have any influence on the porosity and permeability of the soil. It is mainly a chemical process that happens because of the attraction of the molecules of the species to the solid surface. This distinguishes sorption processes from precipitation, which occurs instead when the concentration exceeds the solubility limit of the substance [4].

Desorption is the reverse process of adsorption. It is the release of molecules and ions from the solid phase to the solute [2]. In desorption, the concentration of the chemical species on the solid surface decreases; this is associated with an appropriate increase of the concentration in solution [4].

The relationship between the solute concentration in the adsorbed phase and in the fluid phase is called *adsorption isotherm* [2]. An adsorption isotherm is a function that relates the amount of a species adsorbed on the solid to its amount dissolved in the liquid phase, at a fixed temperature, assuming chemical equilibrium condition between the two quantities [4]. Denoting F as the mass of adsorbed species per unit mass of the solid, the following examples are the most common isotherms in literature [4]:

- Freundlich isotherm

$$F = bc^m \qquad 1.1.17a$$

  where c is the concentration of the adsorbate and b and m are constant coefficients that depend on temperature. $m < 1$ means that as F increases, it becomes difficult for the adsorbate to be adsorbed on a solid. It is the opposite situation when $m > 1$.

- Linear isotherm

$$F = K_d c \qquad 1.1.17b$$

Eq. (1.1.17*b*) is a special case of Freundlich isotherm with $m = 1$. The coefficient K_d expresses the affinity of the substance for the solid and called the *distribution coefficient* or *partitioning coefficient*.

- Langmuir isotherm

$$F = k_1 \frac{k_2 c}{1 + k_2 c} \qquad 1.1.17c$$

where k_1 is a constant that indicates the maximum adsorption fraction which means that, differently from the Freundlich and linear isotherms, Langmuir isotherm involves a maximum adsorption capacity, and k_2 is constant energy coefficient that depends on the adsorbate itself.

1.2 Mineral Precipitation and Inhibition Treatment

Precipitation of organic/inorganic species is a well-known problem that affects the efficiency of wells producing oil, gas and geothermal water. Depending on the type of the porous medium and the fluid, scaling (precipitation of solid material in the near well region) can occur in different forms [1]. While in oil producing wells the main observed precipitation is asphaltene, in geothermal and freshwater wells the precipitation of minerals, (such as, calcium carbonate, calcium sulphate, magnesium and iron compounds) dominates most commonly [1] [6]. In this section we will give an overview of the types and reasons of precipitation, provide a mathematical model to describe the phenomenon and finally present the techniques to prevent the precipitation and the continuous inhibitor injection method. In this thesis the focus is given to inorganic precipitation of mineral salts.

1.2.1 Types of precipitation

Precipitation in reservoirs systems, as well as in near-well region, typically occurs as a result of over-saturation of dissolved species in the fluid flowing within the formation. First, it should be noted that there are several terms in literature to describe the precipitation process, which are: *scaling*, *deposition*, *crystallisation*. In the following, these words will be used equivalently.

Precipitation in the near-well zone can occur in many different forms, but generally it is categorized as organic and inorganic precipitation.

Typical organic precipitates observed in petroleum wells are paraffins and asphaltenes. These are very thick, sticky and deformable substances; therefore, they can clog the pore throats and reduce the permeability to zero without removing the porosity

completely. Their deposition in the reservoir is an irreversible process unless a proper treatment is applied [1].

Being the focus of this thesis, general inorganic precipitation typically includes calcite ($CaCO_3$), gypsum ($CaSO_4$), celestite ($SrSO_4$), magnesium sulphate ($MgSO_4$), some iron compounds with oxygen and sulphur, etc. Typically, precipitation of these minerals is directly related to the concentration of aqueous species in the reservoir fluid. Complex geochemical processes in the reservoir give rise to high concentrations of these species which result in crystallisation in the flowing fluid. Eventually, these crystallised matters are too heavy to stay in the solution and they fall on the solid matrix until the flow paths for groundwater are blocked [6].

Additionally, in literature it is mentioned also biological and physical blockage. Shortly, biological blockage is a slimy deposit composed of bacterial growth. Mineral and biological deposition can occur together, and these formations are referred as biofilm [6]. Physical deposits are usually composed of migrating particles such as sand and clay brought into the near-well region as a result of pumping or the natural movement of the fluid in the reservoir [6].

1.2.2 Causes of precipitation

There are many reasons that cause precipitation in the near-well region, but the primary reason is the quality of the reservoir fluid. Chemical composition of the subsurface fluid is determined by the many factors including the geological structure, minerology and the depth of the reservoir, residence time and exposure to external effects [1] [6] [7]. Focusing on minerals, a classical approach to modelling of precipitation is based on the saturation index (SI). In this approach the precipitation kinetics is proportional to the difference between the concentration of aqueous species and an equilibrium concentration. Assuming a simple system where a single chemical species is considered the SI [-] is defined as

$$SI = \frac{c}{c_{eq}} \qquad 1.2.1$$

The equilibrium concentration is influenced by the reservoir conditions (e.g. temperature), and, in turn, affects the saturation index. When the saturation index exceeds the value of one, the minerals precipitate, as a result, eventually producing the scale by accumulating on the rock solid matrix or to the well structure. The process opposite to precipitation is dissolution, which can occur when the saturation index is less than one. In this case, corrosion of the metal well structure and accumulation of iron oxide as incrustation is observed. Hence, precipitation and dissolution are highly correlated to the saturation index.

Under natural conditions the fluid in the reservoir is in equilibrium: the saturation index is nearly neutral, namely, precipitates are not expected to form, and deposits are not expected to dissolve. Drilling of boreholes to exploit the subsurface fluid, injection to and extraction from the wells cause fluid displacement and consequently a departure from the

equilibrium. The following are the primary factors reported in literature, that affect the aqueous solubility and contribute to high values of saturation index [1] [2] [6] [8]:

- *pH*. Many aqueous constituents are subject to pH effects. Distribution of carbonate species is firmly related to the pH-dependence of solubility of many metals. Important examples among these metals are calcium and magnesium, which are found in the forms as Ca^{2+} and Mg^{2+}, respectively. These two metals form complexes and precipitates with hydroxide, bicarbonate and carbonate [2].
- *Temperature*. Temperature has a crucial role in defining the reaction rates and equilibrium in chemical equations. Even though in general, reaction rates increase with temperature since the thermal energy increases, this phenomenon is not true for some minerals. For instance, minerals such as calcium carbonate and calcium sulphate are less soluble when an increase in temperature happens, and if they are close to the saturation level, this results in precipitation. Most reservoirs are located few hundred meters away from the ground surface, so they do not get influenced by seasonal changes in temperature. Under these conditions, temperature behaves more like a constraint than a variable to define the parameters in chemical and physical equations [2] [6].
- *Velocity change*. Flow velocity can change e.g. due to pumping at production wells and can create an unbalanced state in the reservoir [6].
- *Pressure*. Saturation index is affected by the changes in pressure and off-gassing of dissolved gases as the result of this change. Decrease in pressure at the near-well region is followed by decrease in the equilibrium concentration of the dissolved constitutes. Consequently, in the vicinity of the well reservoir fluids tend to be oversaturated with respect to these species [6].
- *Interaction with an incompatible formation fluid*. This problem occurs due to the mixing of fluids characterized by different chemical signature. This may happen in different situations, for instance close to hydrocarbon extraction wells or within geothermal fields. First, in oil wells extensive use of water injection to maintain the reservoir pressure can have side effects such as scale deposition of calcium, strontium and barium sulphates. Second, in geothermal reservoirs fluids are injected through the injection wells to be heated by geothermal energy in hot, porous rock formations. Then this fluid is extracted from the adjacent pumping wells to generate electricity or directly for geothermal heating. This action can have side effects as the mixing of fluids characterized by different chemical composition can lead to an alteration of the geochemical equilibrium and consequently induce precipitation-dissolution processes [1] [2] [8].

1.2.3 Reservoir remediation techniques

Control and treatment of formation damage due to the precipitation is an important issue to be resolved for efficient use of reservoirs and their economic management. In spite of extensive research and development efforts, effective and reliable method to remediate the formation damage is still a challenging task. Because formation damage is an irreversible process in most cases, the best approach is to prevent it before it happens. Preventative maintenance can save considerable time and cost [1].

Evidently, the performance of the treatment technique depends on the reservoir type and fluid contained in it. Several methods are represented in literature such as clay stabilization, pH buffering, intense heat treatment [1], periodic cleaning of the casing and screen of the well, acid treatment [6], continuous injection of inhibiting species, etc. Designing the right treatment method is an important matter. Soil and fluid type and properties, dissolved species in the fluid, environmental conditions should be examined carefully, and the necessary data should be collected before starting the remediation process.

Focusing on formation damage as a result of mineral precipitation, in this thesis, continuous injection of inhibitors to the reservoir from the borehole is considered. Production stops and the well is treated like an injection well – the fluid (compatible with the reservoir one) is continuously injected for a fixed amount of time from the well-bottom to the reservoir together with the dissolved inhibitor. A part of the inhibitor adsorbs on the solid rock surface preventing the precipitation which is the key point of the inhibitor efficiency. Amount of the inhibitor to be injected, adsorption capacity, the distance that the inhibitor spread from the well-bottom have to be analysed in order to understand how to use the inhibitor treatment efficiently. It is known from the literature that mineral precipitation (calcium sulphate, calcium carbonate) can be treated with inhibitors based on phosphonate and/or polymer compounds [9] [10] [11]. Indeed, the inhibitor is used in the original scenario of the numerical simulation is both phosphonate and polymer based which is a product of CHIMEC S.p.A..

Chapter 2: MATHEMATICAL MODEL

In the recent few decades advanced development of digital computers entailed the use of mathematical and numerical models to predict the dynamic behaviour of subsurface systems. Coupled with boundary conditions, the numerical solution of the equations describing fluid flow and solute transport can provide quantitative information that enables us to understand and utilize reservoir capitals in the best way.

In the next two sections, we will develop a mathematical model, able to capture the key features of the precipitation and inhibition process described in sections 2.1 and 2.2, under some simplifications in the physical and chemical complexity of the problem. The model is solved by means of a numerical algorithm, and a software program is developed to simulate the iterative process of production and injection of inhibitors.

2.1 Model Definition and Assumptions

A deterministic mathematical model of a reservoir generally requires solving a system of partial differential equations (PDE). The number and types of the equations depends on the dominant governing processes. The aim of this work is to simplify the general system of PDEs which will be introduced in the next section, as much as possible, to get a model sufficiently accurate while preserving a reasonable applicability level. As a matter of fact, the numerical solution of this type of system (even if well-known in literature and addressed in several studies, see [12] for instance) could imply a quite extensive computational time, as well as the development of a code very sensitive to several parameters, the latter being usually unknown unless in specific conditions that could be far away from the application in general situations and scenarios. The main model concepts employed in this chapter are derived by former modelling studies dealing with solute transport and remediation techniques in groundwaters (mainly [13] and [14]), readopted to the specific problem by following the general theory of formation damage [1]. The scheme of the near-wellbore zone is depicted in Figure 2.1.1 (the scales in the figure are deformed to facilitate the visualization). The model and the assumptions are described as follows:

- The height H [m] of the well screen (a filtering device that permits the fluid to enter and prevents sediment from entering the well) is much smaller than the radius R [m] of the circular area under consideration, $H<<R$ (see Appendix). The existence of radial symmetry lets us consider one-dimensional radial flow on an imaginary circular plate in the subsurface as

an equation averaged on the height of the screen. This is a fundamental simplification of the problem, even if widely accepted in literature (see [1] [12], for instance).

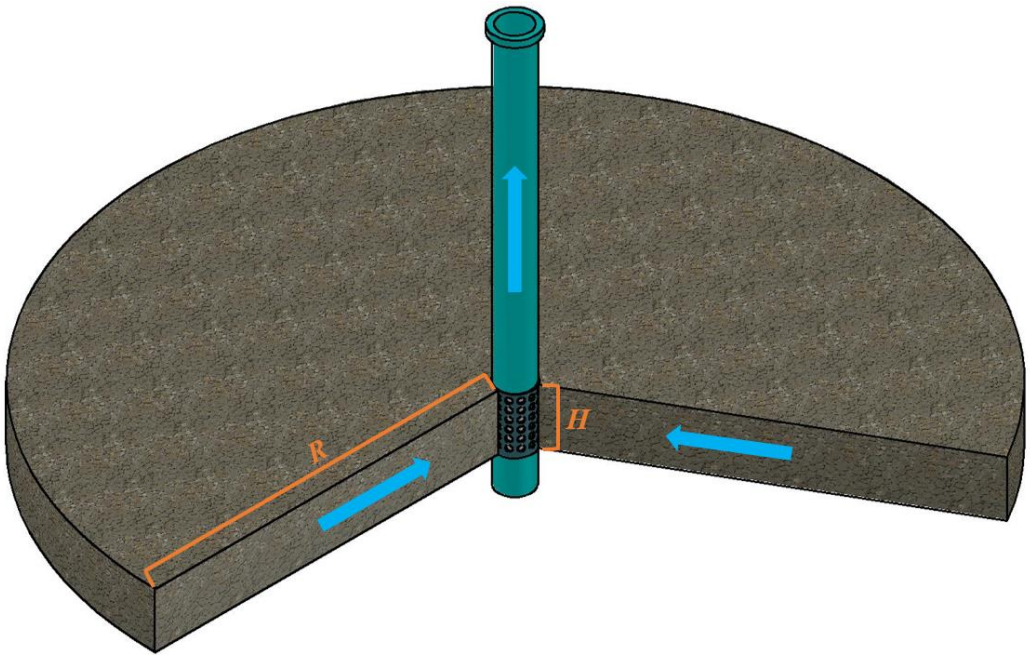

Figure 2.1.1: Conceptual model of the near-wellbore zone

- We assume here a single well model, in other words, either there exists only one well in the field, or other wells existing in the same exploitation field are assumed to be far enough that the discharge and the drawdown of each well will not be affected by neighbouring wells. This assumption allows neglecting any interference to the dynamics of the model due to neighbouring wells.
- The model assumes a single-phase fully saturated homogenous flow, even though the produced fluid from the reservoir is typically a mix of oil, water and dissolved gas, which means that the flow is multiphase.
- Assumption of full penetration (the well screen is completely immersed inside the saturated zone of the reservoir) allows expecting that the well receives fluid from horizontal flow. Note that this assumption is not valid for a partially penetrating well since it induces vertical potential gradients in the reservoir.
- The considered area of the subsurface is far enough from the ground surface (approximately 2 km [9]), so that, this area is not affected by the seasonal changes in temperature, and isothermal conditions can be assumed. The variation of the temperature is estimated to be 1-2 °C different than the annual average temperature which has minor effects on the dynamics of the model. Temperature variation due to geothermal gradient is also negligible due to the average of equations along the vertical direction.

- In this model we define only one precipitating substance (precisely, a mineral salt such as calcium carbonate, calcium sulphate, strontium sulphate, etc.) and thus the selected constitutive laws (e.g. precipitation model) are linked to the kinetics of this matter in the porous medium. In this specific case of mineral salts, it is possible to neglect the influence of the precipitating substance on the fluid density, which therefore is considered always equal to the "pure" fluid density (this assumption, for instance, may not be true in case of asphaltene). The same assumption holds true also for the fluid viscosity.
- Reservoir fluid has a negligible compressibility.
- Assumption that the reservoir is homogenous lets us to have a constant horizontal absolute permeability and porosity over the domain.

Pressure in the near-well region at the bottom hole is the main interest during the production. Assuming a constant production rate, decrease in the bottom-hole pressure indicates the permeability damage in the reservoir. As a result, loss of pressure in the well-bottom is the key output of the model.

The precipitation is controlled by the super-saturation of the dissolved species in the fluid. When the saturation index is higher than one the dissolved concentration in the fluid recovers the equilibrium by precipitating.

It should be pointed out that in the following model only the precipitation is considered; dissolution of the species from the formation rock is not taken into account. If the dissolution is to be regarded, the corresponding system of chemical reaction equations should be solved.

2.2 System of PDEs and Constitutive Laws

As mentioned in the introduction the model represents two scenarios of the process: normal production and production with inhibitor, latter being composed of periodical injection-production process. The complete model consists of a system of PDEs which includes:

- Mass balance equation for the fluid containing precipitating substances,
- Transport equation for the precipitating species dissolved in the fluid,
- Momentum balance equation for the fluid expressed by Darcy's law,
- Transport equation for the concentration of inhibitor,
- A series of constitutive laws and equations expressing the several properties involved (precipitation, porosity and permeability reduction, etc.).

Equations to form this system are taken from previous literature (e.g. [1] [12] [13] [14] [6] [8]).

When mineral precipitation occurs, effective porosity of the medium $\phi(r,t)$ [-] starts reducing [1]:

$$\phi(r,t) = \phi_0 - \varepsilon_p(r,t) \quad 2.2.1$$

where ε_p is the porosity difference (fractional bulk volume) due to precipitation. We define the total density of the flowing fluid, ρ [kg/m^3], as:

$$\rho = \rho_p \sigma_p + (1 - \sigma_p)\rho_f \quad 2.2.2$$

where ρ_p and ρ_f are the density of the precipitating species and the fluid, respectively, and σ_p is the volume fraction corresponding to the precipitation.

Recalling that the fluid density is not affected by the density of the mineral precipitates, $\sigma_p << 1$, we assume $\rho \approx \rho_f$.

Mass balance equation. General mass balance equation for a single-phase homogenous flow in a porous medium is defined as [12]:

$$\frac{\partial(\phi\rho)}{\partial t} = -\nabla \cdot (\rho \mathbf{u}) \quad 2.2.3$$

where **u** [m/s] is the Darcy's flux.

In cylindrical coordinates (r, θ, z) and considering one dimensional radial flow, eq. (2.2.3) takes the form:

$$\phi \frac{\partial \rho}{\partial t} + \rho \frac{\partial \phi}{\partial t} = -\frac{1}{r}\frac{\partial}{\partial r}(r\rho u) \quad 2.2.4$$

where u is the radial component of **u.**

Taking into account eq. (2.2.1) we obtain

$$\phi \frac{\partial \rho}{\partial t} + \frac{1}{r}\frac{\partial}{\partial r}(r\rho u) = \rho \frac{\partial \varepsilon_p}{\partial t} \quad 2.2.5$$

The first term on the left-hand side can be written as:

$$\frac{\partial \rho}{\partial t} = \rho'(p)\frac{\partial p}{\partial t}$$

where p [kg/m/s^2] is the pressure. By calling $\rho'(p) = \beta$, the effective compressibility of the fluid, (2.2.5) reads as

$$\phi\,\beta\frac{\partial p}{\partial t}+\frac{1}{r}\frac{\partial}{\partial r}(r\rho u)=\rho\frac{\partial \varepsilon_p}{\partial t} \qquad 2.2.6$$

The kinetics of the fractional bulk volume ε_p will be defined later.

Momentum balance equation. In addition to eq. (2.2.3), we state the momentum balance equation that can be expressed by Darcy's law. It is worth to note that phenomenon is considered in the range of validity of Darcy's law. This law indicates a linear relationship between the fluid velocity and the *pressure head gradient* [12]:

$$\mathbf{u}=\ -\frac{1}{\mu}\mathbf{k}(\nabla p+\rho g\nabla z) \qquad 2.2.7$$

where μ [Pa s] is the dynamic fluid viscosity, $\mathbf{k}$ [m^2] is the absolute permeability tensor of the porous medium, which is assumed to be in diagonal form for a homogeneous medium, g [m/s^2] is the magnitude of the gravitational acceleration and z [m] is the depth. Neglecting the gradient corresponding to the depth and passing to cylindrical coordinates, we get

$$u=\ -\frac{k}{\mu}\frac{\partial p}{\partial r} \qquad 2.2.8$$

where k is the radial component of the diagonal of $\mathbf{k}$.

Transport equation for dissolved calcite. The main goal of this thesis is to design a model to simulate mineral precipitation in the production wells. Since calcium carbonate is one of the most frequently observed deposition, we will establish a model for this mineral. Calcite precipitation usually depends on the fluid chemical composition (e. g. pH, alkalinity, temperature) as described in section 1.1.2. Since we use the saturation index of calcium carbonate for the modelling process, the model itself can be easily adapted to other mineral precipitations.

Saturation index of dissolved calcite Λ [-] is defined as [8] [15] [16]:

$$\Lambda=\frac{[Ca^{2+}][CO_3^{2-}]}{K_s} \qquad 2.2.9$$

where K_s is the equilibrium constant for the reaction

$$CaCO_3(s)\rightleftarrows Ca^{2+}+CO_3^{2-} \qquad 2.2.10$$

and it is defined as [15]

$$K_s=[Ca^{2+}]_{eq}[CO_3^{2-}]_{eq} \qquad 2.2.11$$

$[Ca^{2+}]$ $\left[CO_3^{2-}\right]$ being the ion activity product (IAP). Strongly depending on temperature, K_s determines the equilibrium, hence, the saturation index Λ [-] of the dissolved substance [8] [14] [6] [15]:

$$\Lambda = \frac{c_p}{c_{eq}} \qquad 2.2.12$$

Values for equilibrium constant K_s are found in [8] [15].

In the following we simplify the geochemistry of the problem and consider a transport-reaction equation for the concentration of dissolved calcite, c_p [mol/m^3], reads as [4]

$$\frac{\partial}{\partial t}(\phi\, c_p) + \nabla \cdot (\phi c_p \mathbf{v}) - \nabla \cdot (\phi\, \mathbf{D} \cdot \nabla c_p) = \phi R_p \qquad 2.2.13$$

where **v** [m/s] is the average velocity field defined as

$$\mathbf{v} = \frac{\mathbf{u}}{\phi} \qquad 2.2.14$$

$\mathbf{D} = \mathbf{D}_{diff} + \mathbf{D}_{disp}$ [m^2/s] is the hydrodynamic dispersion tensor defined as the sum of mechanical dispersion and molecular diffusion. Assuming that diffusive flux is much smaller than the dispersive one, diffusion term is neglected remaining only $\mathbf{D} = \mathbf{D}_{disp}$. Since we model the problem on a symmetric domain, we consider only the *longitudinal dispersion coefficient* D_L

$$D_L = a_L|v|$$

where a_L [m] is the longitudinal dispersivity coefficient and v is the average longitudinal (in our case, radial) component of the average velocity field.

The left-hand-side of the eq. (2.2.13) expresses the transport of dissolved species by means of advection with radial Darcy flux u towards the well and by D_L, the mechanical dispersion.

The right-hand-side represents the sink term which is the precipitation rate in the pore spaces of the reservoir that is to be defined. Dissolution of the solid matrix is not considered, as a result, there is not any source term in eq. (2.2.13).

Advective term in eq. (2.2.13) can be written as:

$$\nabla \cdot (\phi c_p \mathbf{v}) = \phi c_p \nabla \cdot \mathbf{v} + \mathbf{v} \cdot \nabla(\phi c_p)$$

The incompressibility assumption implies that

$$\nabla \cdot \mathbf{v} = 0$$

Eq. (2.2.13) takes then the form in radial coordinates

$$\phi \frac{\partial c_p}{\partial t} + c_p \frac{\partial \phi}{\partial t} + v \frac{\partial}{\partial r}(\phi\, c_p) - \frac{1}{r}\frac{\partial}{\partial r}\left(r\phi\, a_L |v| \frac{\partial c_p}{\partial r}\right) = \phi R_p \qquad 2.2.15$$

The precipitation rate, R_p [mol/m^3/s] is defined as [2] [6] [17] [15]:

$$R_p = k_p S(\Lambda^m - 1) \qquad 2.2.16$$

R_p is proportional to the reaction constant k_p [mol/m^2/s] and the specific surface area S [m^2/m^3] of the pore space.

The exponent m takes various values for different precipitation modes [8] [15] [18]. We assume $m = {}^1/_2$ [18].

The time-rate of change of porosity is proportional to the precipitation rate:

$$\frac{\partial \phi}{\partial t} = -\frac{\partial \varepsilon_p}{\partial t} = -V_s k_p S(\Lambda^m - 1) = V_s R_p \qquad 2.2.17$$

where V_s [m^3/mol] is the molar volume of calcite.

Substituting eq. (2.2.17) in eq. (2.2.15) and rearranging the terms, we obtain the final version of the transport-reaction equation for calcite:

$$\phi \frac{\partial c_p}{\partial t} + v \frac{\partial}{\partial r}(\phi\, c_p) - \frac{1}{r}\frac{\partial}{\partial r}\left(r\phi\, a_L |v| \frac{\partial c_p}{\partial r}\right) = R_p(\phi - c_p V_s) \qquad 2.2.18$$

Moreover, eq. (2.2.17) defines also the time rate of change of the fractional bulk volume which appears in eq. (2.2.6).

The permeability reduction can be represented as an exponential function of the fractional bulk volume (porosity difference) ε_p [1] [5]:

$$k = k(\phi) = k_0 \exp\big(-a(\phi_0 - \phi)\big) = k_0 \exp\big(-a\varepsilon_p\big) \qquad 2.2.19$$

where k_0 [m^2] is the radial component of the diagonal of the initial effective permeability of porous medium and a [-] takes different values according to the soil type. Formation damage happens as a result of two mechanisms: solid surface deposition and pore throat clogging. The reason to choose an exponential relationship is that the pore throat clogging can cause more permeability damage than pore surface deposition and decrease permeability to zero without losing the porosity completely [1].

Transport equation for inhibitor. Modelling the injection of inhibitors requires to consider transport equation for the inhibitor concentration. As noted before, working principle of inhibitors is to adsorb on the solid surface and prevent the precipitation of mineral mechanically. Hence, we need to define an adsorption isotherm for the inhibitor.

Here we assume that the adsorption process can be described by an equilibrium constitutive law. Following the laboratory experiment done in [9], we select Langmuir adsorption-desorption isotherm curve [4]:

$$F = F_{max} \frac{bc_i}{1 + bc_i} \tag{2.2.20}$$

where c_i [kg/m^3] denotes inhibitor concentration in the injection fluid, b [m^3/kg] is inhibitor adsorption energy coefficient, F_{max} [-] is maximum inhibitor adsorption capacity and F is the mass of the adsorbed inhibitor per unit mass of the solid.

Transport equation for the inhibitor concentration expressed in one-dimensional radial coordinates reads as [4]

$$\frac{\partial}{\partial t}(\phi c_i) + v\frac{\partial}{\partial r}(\phi\, c_i) - \frac{1}{r}\frac{\partial}{\partial r}\left(r\phi\, a_L |v| \frac{\partial c_i}{\partial r}\right) = \rho_b \frac{\partial F}{\partial t} \tag{2.2.21}$$

where ρ_b [kg/m^3] is the bulk density of the solid.

The effect of the inhibitor on the precipitation is modelled as the retardation of the precipitation rate, R_p:

$$R_{pi} = \left(1 - \eta \frac{F}{F_{max}}\right)^n R_p \tag{2.2.22}$$

where R_{pi} denotes the precipitation rate under influence of the inhibitor.

Hence the time-rate of change of porosity eq. (2.2.17) is modified accordingly

$$\frac{\partial \phi}{\partial t} = V_s R_{pi} \tag{2.2.23}$$

Since

$$\frac{\partial F}{\partial t} = \frac{\partial F}{\partial c_i}\frac{\partial c_i}{\partial t} = F_{max} \frac{b}{(1 + bc_i)^2}\frac{\partial c_i}{\partial t} \tag{2.2.24}$$

Taking into account eq. (2.2.23) and substituting eq. (2.2.24) in eq. (2.2.21) we obtain:

$$\left(\phi + \rho_b F_{max} \frac{b}{(1 + bc_i)^2}\right)\frac{\partial c_i}{\partial t} + v\frac{\partial}{\partial r}(\phi\, c_i) - \frac{1}{r}\frac{\partial}{\partial r}\left(r\phi\, a_L |v| \frac{\partial c_i}{\partial r}\right) = -c_i V_s R_{pi} \tag{2.2.25}$$

In summary, equations (2.2.6), (2.2.8), (2.2.16), (2.2.17), (2.2.18), (2.2.19), (2.2.25) constitutes the system of PDEs for the whole process.

2.3 Initial and Boundary Conditions

To close the system boundary and initial conditions are required. First of all, let Ω [m] denote the spatial domain and T [s] denote the time domain.

Fixed production rate, Q [m^3/s], is imposed in the well-bottom which is used to calculate the boundary condition for Darcy's flux u_w [m/s]:

$$u(r = r_w) = \frac{Q}{2\pi r_w H} \qquad \forall t \in T \qquad 2.3.1$$

where H [m] is the height of the well screen and r_w [m] is the radius of the well. Note that during production since the fluid flows towards the well, Darcy's flux has negative sign (hence, also the production rate).

Having a fixed Darcy's flux at the well ($r = r_w$) time-dependent Neumann boundary condition is set for the pressure:

$$\frac{\partial p}{\partial t}(r = r_w) = -\frac{\mu}{k} u_w \qquad \forall t \in T \qquad 2.3.2$$

In eq. (2.3.2) time-dependency is due to the decrease in the permeability.

Continuity equation is completed with a fixed Dirichlet boundary condition for pressure in the far boundary of the domain ($r = R$):

$$p(r = r_w) = p_\infty \qquad \forall t \in T \qquad 2.3.3$$

The steady-state solution of the continuity equation with initial constant permeability is accepted as the initial condition:

$$p(t = 0) = steady - state\ solution \qquad \forall r \in \Omega \qquad 2.3.4$$

For the transport equation of the precipitating species at the well $r = r_w$ during the production phase zero-Neuman boundary condition, during the injection of inhibitors constant Dirichlet boundary condition is imposed with saturation index Λ_{pr} whose value is taken from the previous production phase, and Dirichlet boundary condition at $r = R$ represents the equilibrium:

$$\frac{\partial c_p}{\partial t}(r = r_w) = 0 \qquad (production) \qquad \forall t \in T \qquad 2.3.5$$

$$c_p(r = r_w) = \Lambda_{pr} c_{eq} \qquad (injection) \qquad \forall t \in T \qquad 2.3.6$$

$$c_p(r = R) = c_{eq} \qquad \forall t \in T \qquad 2.3.7$$

To ensure a smooth decay of the concentration of the precipitation and to satisfy the homogenous Neumann boundary condition at the well, parabolic behaviour is chosen as initial condition:

$$c_p(t=0) = \frac{\Lambda_i c_{eq}}{R^2}(r^2 - R^2) + c_{eq} \qquad \forall r \in \Omega \qquad 2.3.8$$

where Λ_i represents the initial saturation index at the well.

For the transport equation of inhibitor concentration boundary condition at the well is imposed in the similar way of the precipitation; constant Dirichlet boundary condition during the injection and homogeneous Neuman boundary condition during the production:

$$c_i(r = r_w) = c_{ifixed} \quad (injection) \qquad \forall t \in T \qquad 2.3.9$$

$$\frac{\partial c_i}{\partial t}(r = r_w) = 0 \qquad (production) \qquad \forall t \in T \qquad 2.3.10$$

At $r = R$ homogeneous Dirichlet boundary condition is set:

$$c_i(r = R) = 0 \qquad \forall t \in T \qquad 2.3.11$$

The initial condition of the inhibitor is zero for the whole domain:

$$c_i(t = 0) = 0 \qquad \forall r \in \Omega \qquad 2.3.12$$

2.4 Dimensionless Equations

For better understanding the dynamics of the system and the scales of the individual processes we will use dimensionless variables to solve the equations. Defining $\hat{P}$, $\hat{U}$, $\hat{K}$, $\hat{C}$, $\hat{C}_i$, $\hat{T}$, $\hat{R}$ as the characteristic values of pressure, Darcy's flux, permeability, precipitation concentration, inhibitor concentration, time and radius, respectively, the equations can be rewritten as follows:

Continuity equation (2.2.6) takes the form (note that equations (2.2.8) and (2.2.17) are substituted in eq. (2.2.6)):

$$\frac{\hat{P}}{\hat{T}}\phi\beta\frac{\partial p^*}{\partial t^*} - \frac{\hat{P}\hat{K}}{\hat{R}^2}\frac{\rho}{\mu}\frac{1}{r^*}\frac{\partial}{\partial r^*}\left(r^* k^* \frac{\partial p^*}{\partial r^*}\right) = -\rho V_s R_p \qquad 2.4.1$$

where the precipitation rate is:

$$R_p = -k_p S\left(\Lambda^{1/2} - 1\right) \tag{2.4.2}$$

Momentum balance equation in dimensionless form reads as:

$$u^* = \frac{\hat{P}\hat{K}}{\hat{U}\hat{R}\mu} k^* \frac{\partial p^*}{\partial r^*} \tag{2.4.3}$$

Dimensionless transport-reaction equation (2.2.18) for the concentration of calcite is:

$$\frac{\hat{C}}{\hat{T}}\phi\frac{\partial c_p^*}{\partial t^*} + \frac{\hat{C}\hat{U}}{\hat{R}} v^* \frac{\partial}{\partial r^*}\left(\phi c_p^*\right) - \frac{\hat{C}\hat{U}a_L}{\hat{R}^2}\frac{1}{r^*}\frac{\partial}{\partial r^*}\left(r^*\phi|v^*|\frac{\partial c_p^*}{\partial r^*}\right) = R_p\left(\phi - \hat{C}c_p^* V_s\right) \tag{2.4.4}$$

Dimensionless transport equation (2.2.25) for the concentration of the inhibitor reads as:

$$\left(\phi + \rho_b F_{max}\frac{b}{\left(1 + b\widehat{C}_\iota c_i^*\right)^2}\right)\frac{\widehat{C}_\iota}{\hat{T}}\frac{\partial c_i^*}{\partial t^*} + \frac{\widehat{C}_\iota\hat{U}}{\hat{R}} v^* \frac{\partial}{\partial r^*}\left(\phi c_i^*\right) - \frac{\widehat{C}_\iota\hat{U}a_L}{\hat{R}^2}\frac{1}{r^*}\frac{\partial}{\partial r^*}\left(r^*\phi|v^*|\frac{\partial c_i^*}{\partial r^*}\right) = -\widehat{C}_\iota c_i^* V_s R_{pi} \tag{2.4.5}$$

where R_{pi} is defined by (2.2.22).

Permeability decrease in dimensionless form is:

$$k^* = \frac{k_0}{\hat{K}}\exp\left(-a\varepsilon_p\right) \tag{2.4.6}$$

Also, the boundary conditions are scaled accordingly (not reported here).

2.5 More on the Pressure Equation

We perform a careful sensitivity analysis on the pressure eq. (2.4.1) in order to understand the scales between transient, diffusion and reaction terms. In particular, we

want to observe if it is possible to neglect the transient and the reaction terms, so that we can solve the eq. (2.4.1) analytically. We define from the eq. (2.4.1):

Transient term coefficient:

$$T_p = \frac{\hat{P}}{\hat{T}}\phi\beta$$

Diffusion term coefficient:

$$D_p = \frac{\hat{P}\hat{K}}{\hat{R}^2}\frac{\rho}{\mu}$$

Source term coefficient:

$$S_p = \rho V_s k_p S$$

We substitute these coefficients in eq. (2.4.1):

$$T_p \frac{\partial p^*}{\partial t^*} - D_p \frac{1}{r^*}\frac{\partial}{\partial r^*}\left(r^* k^* \frac{\partial p^*}{\partial r^*}\right) = -S_p(\Lambda^m - 1) \qquad 2.5.1$$

By setting different values for characteristic quantities we have examined if it is possible to neglect the transient and reaction term, thus retrieving a stationary equation. In Table 2.1, it is seen the ratio of transient to diffusion, and reaction to diffusion term. The first row is the reference values that are used in the numerical simulation (the values of the parameters that are not shown in the table can be found in Appendix). The results show that transient and reaction terms are almost in the same order. From the results, we decided to neglect these two terms leaving only diffusion of pressure which ends up in steady-state pressure equation that can be solved analytically with the given boundary conditions.

Then the steady-state pressure equation (eq. 2.4.1) reads as:

$$-\frac{\hat{P}\hat{K}}{\hat{R}^2}\frac{\rho}{\mu}\frac{k^*}{r^*}\frac{\partial}{\partial r^*}\left(r^*\frac{\partial p^*}{\partial r^*}\right) = 0 \qquad 2.5.2$$

Solved analytically with the reported boundary conditions we obtain the dimensionless pressure:

$$p^* = \frac{\hat{R}\hat{U}}{\hat{P}\hat{K}}\frac{\mu}{k^*} r_w^* u_w^* \left(\ln\frac{R^*}{r^*}\right) + p_\infty^* \qquad 2.5.3$$

In this case, also the Darcy flux can be solved analytically with varying permeability. The analytical Darcy flux (in dimensionless form) can be obtained:

$$u^* = r_w^* u_w^* \left(\frac{1}{r^*} + \frac{\partial k^*}{\partial r^*} \frac{\ln R^* - \ln r^*}{k^*} \right) \qquad 2.5.4$$

Also considering that the effective compressibility β of the fluid is a very small quantity, we can accept the fluid as incompressible.

$\hat{P}\ [bar]$	$\hat{R}\ [m]$	$\hat{T}\ [day]$	$\hat{K}\ [m^2]$	$\phi\ [-]$	T_p/D_p	S_p/D_p	Steady State?
137	10	30	30e-15	0.27	3.5e-6	9e-6	yes
137	10	30	30e-10	0.27	3.5e-11	9e-11	yes
137	10	30	30e-20	0.27	3.5e-1	9e-1	no
137	2	30	30e-15	0.27	1.4e-7	3.6e-7	yes
137	50	30	30e-15	0.27	8.7e-5	2e-4	no
137	10	30	30e-15	0.10	1.3e-6	9e-6	yes
137	10	30	30e-15	0.60	7e-7	9e-6	yes
137	10	1	30e-15	0.27	2e-4	9e-6	no
137	10	365	30e-15	0.27	2.9e-7	9e-6	yes
10	10	30	30e-15	0.27	3.5e-6	1e-4	no
300	10	30	30e-15	0.27	3.5e-6	4e-6	yes

Table 2.1: Sensitivity analysis of the continuity equation. The red values indicate that the transient and/or the reaction term is not negligible.

Chapter 3: NUMERICAL MODEL

Based on the mathematical model numerical methods yield approximate solutions through the discretization of time and space. Derivative approximations, the scale of discretization, and the matrix solution techniques can lead to significant errors if not properly established.

In the following, the numerical simulation algorithm based on the dimensionless equations introduced in the previous chapter is described. The solution algorithm and the code architecture are detailed. The complete model relies on a finite difference method.

3.1 Numerical Methods for the Equations

Numerical model is represented by finite difference (FD) method and the corresponding code is written in Python 3.

The radial spatial domain is represented (Fig. 3.1.1) by a non-uniform grid with increasing grid size starting from the well r_0, and forming a geometric sequence where $\Delta r_j = \alpha \Delta r_{j-1}$ or $\Delta r_j = \alpha^{j-1} \Delta r_0$ where $\alpha > 1$, $j = 1 : M - 1$. The reason for the choice of this kind of domain discretization is that a detailed information is needed at the near-well region, while in the far boundary it is not necessary, and in this way the simulation time is greatly decreased with respect to the case of a uniform grid with the appropriate resolution for the near-well region.

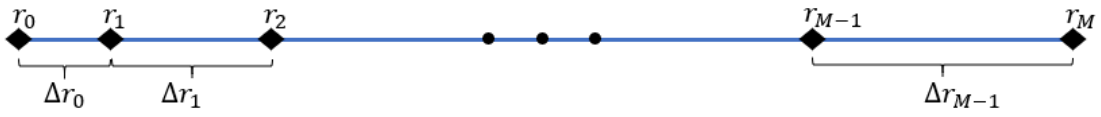

Figure 3.1.1: Discretized spatial domain

Derivation of the discrete derivatives on a non-uniform grid. Following the procedure presented in [19] the discrete derivatives are constructed as below:

Consider an analytical function $f(r)$ in the interval $0 \leq r \leq R$ with $f_j = f(r_j)$. To express the discrete first and second derivatives of f, we expand f_{j+1} and f_{j-1} in Taylor series about the point r_j:

$$f_{j+1} = f_j + \Delta r_j \frac{\partial f}{\partial r_j} + \frac{\Delta r_j^2}{2}\frac{\partial^2 f}{\partial r_j^2} + \frac{\Delta r_j^3}{6}\frac{\partial^3 f}{\partial r_j^3} + \cdots \quad 3.1.1$$

$$f_{j-1} = f_j - \Delta r_{j-1} \frac{\partial f}{\partial r_j} + \frac{\Delta r_{j-1}^2}{2}\frac{\partial^2 f}{\partial r_j^2} - \frac{\Delta r_{j-1}^3}{6}\frac{\partial^3 f}{\partial r_j^3} + \cdots \quad 3.1.2$$

$\frac{\partial f}{\partial r_j}$ and $\frac{\partial^2 f}{\partial r_j^2}$ are the two unknowns to be calculated. The higher order derivatives are also unknown, but we accept the error involved in neglecting them.

To find $\frac{\partial f}{\partial r_j}$ take

$$\Delta r_{j-1}^2 \times (3.1.1) - \Delta r_j^2 \times (3.1.2)$$

to get

$$\frac{\partial f}{\partial r_j} = \frac{f_{j+1}\Delta r_{j-1}^2 + f_j\left(\Delta r_j^2 - \Delta r_{j-1}^2\right) - f_{j-1}\Delta r_j^2}{\Delta r_{j-1}\,\Delta r_j\,(\Delta r_{j-1} + \Delta r_j)} \quad 3.1.3$$

To find $\frac{\partial^2 f}{\partial r_j^2}$ take

$$\Delta r_{j-1} \times (3.1.1) + \Delta r_j \times (3.1.2)$$

to get

$$\frac{\partial^2 f}{\partial r_j^2} = \frac{f_{j+1}\Delta r_{j-1} - f_j\left(\Delta r_j + \Delta r_j\right) + f_{j-1}\Delta r_j}{\Delta r_{j-1}\,\Delta r_j\,(\Delta r_{j-1} + \Delta r_j)/2} \quad 3.1.4$$

The discrete derivatives constructed in this way gives the same accuracy as the uniform grid when the centred difference method is used. In fact, in the case of uniform grid, namely, $\Delta r_{j-1} = \Delta r_j = \Delta r$, (3.1.3) and (3.1.4) reduce to

$$\frac{\partial f}{\partial r_j} = \frac{f_{j+1} - f_{j-1}}{2\Delta r} \quad 3.1.5$$

$$\frac{\partial f}{\partial r_j} = \frac{f_{j+1} + 2f_j - f_{j-1}}{\Delta r^2} \quad 3.1.6$$

Discretization of the model equations. Both transport equations (2.4.4) and (2.4.5) are calculated with Implicit Euler Method for the time derivative.

Transport-reaction equation for the concentration of the precipitating substance. To implement the numerical discretization to eq. (2.4.4) we must simplify the radial derivatives (the symbol $*$ is dropped for simplicity):

$$\frac{\hat{C}}{\hat{T}}\phi\frac{\partial c_p}{\partial t} + \frac{\hat{C}\hat{U}}{\hat{R}}v\left(\phi\frac{\partial c_p}{\partial r} + c_p\frac{\partial \phi}{\partial r}\right) -$$

$$\frac{\hat{C}\hat{U}a_L}{\hat{R}^2}\left(\phi|v|\frac{\partial^2 c_p}{\partial r^2} + \phi\frac{\partial v}{\partial r}\frac{\partial c_p}{\partial r} + |v|\frac{\partial \phi}{\partial r}\frac{\partial c_p}{\partial r} + \frac{\phi|v|}{r}\frac{\partial c_p}{\partial r}\right) =$$

$$-k_p S\left(\Lambda^{1/2} - 1\right)\left(\phi - V_s\hat{C}c_p\right) \qquad 3.1.7$$

Let us call

$$T = \frac{\hat{C}}{\hat{T}} \qquad U = \frac{\hat{C}\,\hat{U}}{\hat{R}} \qquad D = \frac{\hat{C}\,\hat{U}a_L}{\hat{R}^2}$$

The terms with the first derivative of the concentration, derived from the diffusion term as a result of radial representation, namely,

$$\phi\frac{\partial v}{\partial r}\frac{\partial c_p}{\partial r} + |v|\frac{\partial \phi}{\partial r}\frac{\partial c_p}{\partial r} + \frac{\phi|v|}{r}\frac{\partial c_p}{\partial r}$$

behave like advection. Rearranging the terms, eq. (3.1.7) is rewritten as

$$T\,\phi\frac{\partial}{\partial t}(c_p) + Uv\frac{\partial \phi}{\partial r}\,c_p + \left(Uv\phi - D\left(\phi\frac{\partial v}{\partial r} + |v|\frac{\partial \phi}{\partial r} + \frac{\phi|v|}{r}\right)\right)\frac{\partial c_p}{\partial r} -$$

$$D\phi v\,\frac{\partial^2 c_p}{\partial r^2} = -\,k_p S\left(\Lambda^{1/2} - 1\right)\left(\phi - V_s\,\hat{C}c_p\right) \qquad 3.1.8$$

We call

$$a = Uv\phi - D\left(\phi\frac{\partial v}{\partial r} + |v|\frac{\partial \phi}{\partial r} + \frac{\phi|v|}{r}\right) \qquad 3.1.9a$$

$$w = Uv\frac{\partial \phi}{\partial r} \qquad 3.1.9b$$

Discrete forms of a and w are obtained using (3.1.3) and (3.1.4) and presented below:

$$a_j = Uv_j\phi_j - D\left(\phi_j\frac{v_{j+1}\,\Delta r_{j-1}^2 + v_j\left(\Delta r_j^2 - \Delta r_{j-1}^2\right) - v_{j-1}\Delta r_j^2}{\Delta r_{j-1}\,\Delta r_j\,(\Delta r_{j-1} + \Delta r_j)} + \right.$$

$$\left.|v_j|\frac{\phi_{j+1}\Delta r_{j-1}^2 + \phi_j(\Delta r_j^2 - \Delta r_{j-1}^2) - \phi_{j-1}\Delta r_j^2}{\Delta r_{j-1}\,\Delta r_j\,(\Delta r_{j-1} + \Delta r_j)} + \frac{\phi_j\,|v_j|}{r_j}\right) \qquad 3.1.10a$$

$$w_j = Uv_j \frac{\phi_{j+1}\Delta r_{j-1}^2 + \phi_j(\Delta r_j^2 - \Delta r_{j-1}^2) - \phi_{j-1}\Delta r_j^2}{\Delta r_{j-1}\,\Delta r_j\,(\Delta r_{j-1} + \Delta r_j)} \qquad 3.1.10b$$

Then, fully discretized equation reads as

$$T\phi_j^i \frac{c_j^{i+1} - c_j^i}{\Delta t} + w_j^i c_j^{i+1} + a_j \frac{c_{j+1}^{i+1}\Delta r_{j-1}^2 + c_j^{i+1}(\Delta r_j^2 - \Delta r_{j-1}^2) - c_{j-1}^{i+1}\Delta r_j^2}{\Delta r_{j-1}\,\Delta r_j\,(\Delta r_{j-1} + \Delta r_j)} -$$

$$D\,\phi_j^i |v_j^i| \frac{c_{j+1}^{i+1}\Delta r_{j-1} - c_j^{i+1}(\Delta r_j + \Delta r_{j-1}) + c_{j-1}^{i+1}\Delta r_j}{\frac{\Delta r_{j-1}\Delta r_j(\Delta r_j + \Delta r_{j-1})}{2}} = S_j^i \qquad 3.1.11$$

where S_j^i is the sink term that represents the mineral precipitation. Since this term is non-linear we represent it with an explicit approach:

$$S_j^i = -k_p S\left(\Lambda_j^{1/2} - 1\right)\left(\phi_j^i - V_s \hat{C} c_j^i\right)\left(1 - \eta \frac{F_j^i}{F_{max}}\right)^n \qquad 3.1.12$$

The last parenthesis represents the influence of the inhibitor on the precipitation. During the normal production since the inhibitor is not present in the reservoir, F_j^i is zero.

Matrix representation for eq. (3.1.11) is as follows:

$$\left(\mathbf{I} + \frac{\Delta t}{T\phi}(\mathbf{WI} + \mathbf{A} + \mathbf{D})\right)\mathbf{C}^{i+1} = \mathbf{C}^i + \frac{\Delta t}{T\phi}\mathbf{S}^i \qquad 3.1.13$$

where $\mathbf{C}^i$ and $\mathbf{C}^{i+1}$ are the vectors of concentration of calcite at time i and $i+1$, respectively. $\mathbf{I}$ is the identity matrix, $\mathbf{W}$ is the coefficient vector related to w_j^i, $\mathbf{A}$ is the advection matrix, and $\mathbf{D}$ is the diffusion matrix. It must be pointed out that all the matrices and the parameters (e.g., porosity) are updated at every iteration since they depend on the solution itself, and $\mathbf{S}^i$ is the sink term vector at time i. Eq. (3.1.13) is defined inside the domain; $j = 1 : M - 1$, and the matrices and the right-hand-side of the eq. (3.1.13) are modified accordingly when the boundary conditions are added.

The j[th] row in the advection matrix $\mathbf{A}$ reads as

$$\mathbf{A}_j = \left[0 \cdots \quad -\frac{a_j\,\Delta r_j}{\Delta r_{j-1}(\Delta r_{j-1} + \Delta r_j)} \quad \frac{a_j\,(\Delta r_j - \Delta r_{j-1})}{\Delta r_{j-1}\Delta r_j} \quad \frac{a_j\,\Delta r_{j-1}}{\Delta r_j(\Delta r_{j-1} + \Delta r_j)} \quad \cdots 0\right]$$

The j[th] row in the diffusion matrix $\mathbf{D}$ reads as

$$\mathbf{D}_j = \begin{bmatrix} 0 \cdots & -\dfrac{2D\phi_j^i|v_j^i|}{\Delta r_{j-1}(\Delta r_j + \Delta r_{j-1})} & \dfrac{2D\phi_j^i|v_j^i|}{\Delta r_{j-1}\Delta r_j} & -\dfrac{2D\phi_j^i|v_j^i|}{\Delta r_j(\Delta r_j + \Delta r_{j-1})} & \cdots 0 \end{bmatrix}$$

Boundary conditions are imposed as defined in section 2.3. During both production and injection phases Dirichlet boundary condition $c_M = c_R$ is applied on the far boundary $r = r_M = R$. So, the last node $r = r_{M-1}$ of the right-hand-side of eq. (3.1.13) takes the following form with the contribution of the Dirichlet boundary condition:

$$C_{M-1}^i + \frac{\Delta t}{T\phi_{M-1}^i} S_{M-1}^i + \underbrace{\frac{\Delta t}{T\phi_{M-1}^i}\left(-\frac{a_{M-1}\Delta r_{M-2}}{\Delta r_{M-1}(\Delta r_{M-2} + \Delta r_{M-1})} + \frac{2D\phi_{M-1}^i|v_{M-1}^i|}{\Delta r_{M-1}(\Delta r_{M-1} + \Delta r_{M-2})}\right) C_M}_{\text{Contribution of Dirichlet BC at } r = r_M}$$

During the injection at the well $r = r_0 = r_{well}$ Dirichlet boundary condition $c_0 = c_{well}$ is imposed. Hence, the first node $r = r_1$ of the right-hand-side of eq. (3.1.13) is in following form with the contribution of the Dirichlet boundary condition:

$$C_1^i + \frac{\Delta t}{T\phi_1^i} S_1^i + \underbrace{\frac{\Delta t}{T\phi_1^i}\left(\frac{a_1\Delta r_1}{\Delta r_0(\Delta r_0 + \Delta r_1)} + \frac{2D\phi_1^i|v_1^i|}{\Delta r_1(\Delta r_1 + \Delta r_2)}\right) C_0}_{\text{Contribution of Dirichlet BC at } r = r_0}$$

When production is performed zero-Neumann boundary condition is applied at the well and since c_0 is unknown in this case, the zeroth node $r = r_0$ is added in the matrices, and the corresponding lines and columns are constructed accordingly:

$$\mathbf{A}_0 = \begin{bmatrix} 0 \cdots & 0 & \cdots 0 \end{bmatrix}$$

$$\mathbf{D}_0 = \begin{bmatrix} \dfrac{2D\phi_0^i|v_0^i|}{{\Delta r_0}^2} & -\dfrac{2D\phi_0^i|v_0^i|}{{\Delta r_0}^2} & \cdots 0 \end{bmatrix}$$

Transport equation for the concentration of the inhibitor. Discretization of eq. (2.4.5) is implemented in the same way as eq. (2.4.4). We make the necessary simplifications on the radial derivatives as they were done for eq. (2.4.4). Advective flux and the contribution of the porosity variation (a and w) are the same and discretized a_j and w_j reads as in (3.1.10a) and (3.1.10b). However, time variation and the sink term differ. The non-linear terms in the eq. (2.4.4) are dealt with by discretizing with an explicit time scheme. We redefine the transient, advective and diffusive coefficients with the characteristic value of the inhibitor concentration

$$T = \frac{\widehat{C}_\iota}{\widehat{T}} \qquad U = \frac{\widehat{C}_\iota \widehat{U}}{\widehat{R}} \qquad D = \frac{\widehat{C}_\iota \widehat{U} a_L}{\widehat{R}^2}$$

As a result, discretized form of eq. (2.4.5) reads as

$$\left(\phi_j + \rho_b F_{max}\frac{b}{\left(1+b\widehat{C}_\iota c_j^i\right)^2}\right)T\frac{c_j^{i+1}-c_j^i}{\Delta t} + w_j^i\, c_j^{i+1} + a_j\frac{c_{j+1}^{i+1}\Delta r_{j-1}^2 + c_j^{i+1}\left(\Delta r_j^2 - \Delta r_{j-1}^2\right) - c_{j-1}^{i+1}\Delta r_j^2}{\Delta r_{j-1}\Delta r_j(\Delta r_{j-1}+\Delta r_j)} - D\phi_j\left|v_j^i\right|\frac{c_{j+1}^{i+1}\Delta r_{j-1} - c_j^{i+1}\left(\Delta r_j + \Delta r_{j-1}\right) + c_{j-1}^{i+1}\Delta r_j}{\frac{\Delta r_{j-1}\Delta r_j\left(\Delta r_j+\Delta r_{j-1}\right)}{2}} = S_j^i \quad 3.1.14$$

where

$$S_j^i = -V_s\, k_p S\widehat{C}_\iota c_j^i\left(\Lambda_j{}^{1/2}-1\right)\left(1 - \eta\frac{F_j^i}{F_{max}}\right)^n \quad 3.1.15$$

and where

$$F_j^i = F_{max}\frac{bc_j^i}{1+bc_j^i} \quad 3.1.16$$

Matrix representation for eq. (3.1.14) is as follows:

$$\left(\mathbf{I} + \frac{\Delta t}{\mathbf{T}_{cf}}(\mathbf{WI} + \mathbf{A} + \mathbf{D})\right)\mathbf{C}^{i+1} = \mathbf{C}^i + \frac{\Delta t}{\mathbf{T}_{cf}}\mathbf{S}^i \quad 3.1.17$$

where

$$\mathbf{T}_{cf} = T\left(\phi + \rho_b F_{max}\frac{b}{\left(1+b\widehat{C}_\iota\,\mathbf{C}^i\right)^2}\right) \quad 3.1.18$$

Boundary conditions (defined in section 2.3) are added to the eq. (3.1.14) as it was applied for the equation of the precipitating substance.

Porosity and permeability change as a result of precipitation. Porosity variation is calculated through the discretized form of eq. (2.2.17), $j = 1:\ M-1$:

$$\phi_j^{i+1} = \phi_j^i + \Delta t\left(-V_s\, k_p S\left(\Lambda_j{}^{1/2}-1\right)\left(1 - \eta\frac{F_j^i}{F_{max}}\right)^n\right) \quad 3.1.19$$

$\left(1 - \eta\frac{F_j^i}{F_{max}}\right)^n$ is the retardation factor for the precipitation rate (and to the porosity decrease) and it is equal to unity during the normal production since F_j^i is zero (no inhibitor in the domain).

Using the result of the eq. (3.1.19) we calculate the dimensionless permeability through the eq. (2.4.6):

$$k_j^i = \frac{k_0}{\widehat{K}} \exp\left(-a\left(\phi_j^0 - \phi_j^i\right)\right) \qquad j = 1 : M-1 \qquad 3.1.20$$

3.2 Stability Analysis of the Explicit Euler Method

Explicit (Forward) and Implicit (Backward) methods are among the most used approaches applied in solving the time-dependent differential equations numerically. Both of them have their own advantages and disadvantages. It is known that Implicit Euler Method (IEM) is unconditionally stable with respect to the time-step size [20], but accompanied by a loss of accuracy, and usually requires the inversion of the stiffness matrix. On the contrary, Explicit Euler Method (EEM) offers a reduction of the computational complexity, while implies a very restrictive stability condition on the time-step size, which is called CFL (Courant-Friedrichs-Lewy) condition. Thus, the optimal choice between explicit and implicit schemes depends on the problem itself.

In this section we study the stability analysis of the EEM to endorse the choice of IEM for our model. In particular, the stability analysis is performed with a simplified problem, namely, on a uniform Cartesian grid with constant coefficients. The analysis with cartesian coordinates gives an order of magnitude of the CFL condition for our original problem with radial coordinates.

First, let us write the general transport equation for the concentration of a solute c in a porous medium with constant porosity ϕ, in one-dimensional cartesian coordinates, with constant average velocity v and constant diffusivity μ:

$$\phi \frac{\partial c}{\partial t} + v\phi \frac{\partial c}{\partial x} - \mu\phi \frac{\partial^2 c}{\partial x^2} = f \qquad 3.2.1$$

where f is the source/sink term.

By discretizing this equation with explicit centred method (we choose centred difference method since we used implicit centred method in the previous section) in a uniform grid with Δx grid size, we get:

$$\phi \frac{c_j^{i+1} - c_j^i}{\Delta t} + v\phi \frac{c_{j+1}^i - c_{j-1}^i}{2\Delta x} - \mu\phi \frac{c_{j+1}^i - 2c_j^i + c_{j-1}^i}{\Delta x^2} = f_j^i \qquad 3.2.2$$

In matrix representation:

$$\mathbf{c}^{i+1} = \left(\mathbf{I} + \Delta t(\mathbf{A} + \mathbf{D})\right)\mathbf{c}^i + \Delta t\, \mathbf{f}^i \qquad 3.2.3$$

where

$$\mathbf{A}_j = \left[0 \cdots \quad \phi\frac{a}{2\Delta x} \qquad 0 \qquad -\phi\frac{a}{2\Delta x} \quad \cdots 0\right]$$

and

$$\mathbf{D}_j = \left[0 \cdots \quad \phi\frac{\mu}{\Delta x^2} \qquad -\phi\frac{2\mu}{\Delta x^2} \qquad \phi\frac{\mu}{\Delta x^2} \quad \cdots 0\right]$$

To analyse the stability condition we follow the methods described in literature [20] [21] [22]. Let $f = 0$, and we define a suitable norm:

$$\| \mathbf{c} \|_{\Delta,p} = \left(\Delta x \sum_{j=1}^{N-1} |c_j|^p\right)^{1/p} \quad p = 1, 2 \qquad 3.2.4$$

Absolute stability requires that [20]

$$\left\|\mathbf{c}^{i+1}\right\|_{\Delta,p} \leq \left\|\mathbf{c}^{i}\right\|_{\Delta,p} \qquad 3.2.5$$

This is guaranteed if

$$\|\mathbf{I} + \Delta t(\mathbf{A} + \mathbf{D})\| \leq 1 \qquad 3.2.6$$

The norm of a matrix can be calculated with its largest eigenvalue that can be found numerically. However, here a simpler approach which is defined in [21] is applied to find the following CFL condition for the eq. (3.2.2):

$$\Delta t \leq \frac{\Delta x^2}{a\Delta x + 2\mu} \qquad 3.2.7$$

This condition is verified also with numerical simulations. Indeed, when the numerical simulation is run with the original parameters (porosity, average velocity, dispersivity) with $\Delta x = 0.1$ m, maximum time-step size must be fixed at a value less than 60 seconds to maintain the stability. This is a very small amount considering that the total simulation time is close to 10 years, which makes EEM unfeasible for our model.

3.3 Convergence Criteria

To find an estimation of the uncertainty due to the numerical discretization of the problem, convergence property is analysed through a procedure which is introduced in [23] and [24]. We cannot perform a rigorous convergence analysis since there is no analytical solution for our problem.

The recommended method for discretization error estimation is the Richardson extrapolation (RE) method which is based on the *Grid Convergence Index* (GCI). The procedure is described as below:

Step 1. Define a representative mesh size Δr:

$$\Delta r = \frac{1}{M}\sum_{i=1}^{M}\Delta r_i \qquad 3.3.1$$

where Δr_i is the length of the ith cell and M is the total number of the cells used for the computations.

Step 2. Select three different sets of grids and run simulations to determine the values of the variables. It is desirable that the grid refinement factor $\tau = \Delta r_{coarse}/\Delta r_{fine}$ to be greater than 1.3. This value is based on previous experience and not on formal derivation.

Step 3. Let φ be a variable of interest and $\Delta r_1 < \Delta r_2 < \Delta r_3$ and $\tau_{21} = \Delta r_2/\Delta r_1$, $\tau_{32} = \Delta r_3/\Delta r_2$. We can calculate the apparent order q of the method using:

$$q = \frac{1}{\ln(\tau_{21})}\left|\ln|\varepsilon_{32}/\varepsilon_{21}| + p(q)\right| \qquad 3.3.2a$$

$$p(q) = \ln\left(\frac{\tau_{21}^{q} - s}{\tau_{32}^{q} - s}\right) \qquad 3.3.2b$$

$$s = 1 \cdot \mathrm{sgn}\left(\frac{\varepsilon_{32}}{\varepsilon_{21}}\right) \qquad 3.3.2c$$

where $\varepsilon_{21} = \varphi_2 - \varphi_1$, $\varepsilon_{32} = \varphi_3 - \varphi_2$ and φ_k denotes the solution on the kth grid. The system (3.3.2) can be solved through the fixed-point iteration method, with the initial guess equal to the first term in eq. (3.3.2*a*). Moreover, it should be noted that if either ε_{21} or ε_{32} is very close to zero (meaning that φ_1, φ_2 and φ_3 are very close to each other), the above procedure does not work.

Step 4. Calculate the extrapolated values:

$$\varphi_{ext}^{21} = \frac{\tau_{21}^{q}\varphi_1 - \varphi_2}{\tau_{21}^{q} - 1} \qquad 3.3.3$$

similarly, calculate φ_{ext}^{32}.

Step 5. Calculate the relative errors:

$$e^{21} = \left|\frac{\varphi_1 - \varphi_2}{\varphi_1}\right|, \quad e_{ext}^{21} = \left|\frac{\varphi_{ext}^{21} - \varphi_1}{\varphi_{ext}^{21}}\right| \qquad 3.3.4$$

and the Grid Convergence Index:

$$\mathrm{GCI}^{21} = \frac{F_s\, e^{21}}{\tau_{21}^{q} - 1} \qquad 3.3.5$$

which approximates the relative error between fine-grid and coarse-grid solutions. It indicates how much the solution would change with a further refinement of the grid. F_s is interpreted as a safety factor and is recommended to be 3.0 for comparison of two grids and 1.25 for comparison of three or more grids [24].

3.4 Solution Set-up

We describe in the following the set-up of the simulation employed in the numerical results reported in Chapter 4. As previously mentioned, the numerical model simulates two scenarios: *normal production* and *production with inhibitor*. Fig 3.4.1 shows the set-up of the simulation. The solution of the steady-state continuity eq. (2.5.3) and the analytical Darcy's flux (2.5.4) with initial constant permeability and porosity is taken as an initial condition for both scenarios. We perform the simulations as follows:

a) *Normal production (NP):* Fluid flows towards the well (thus fluid velocity has a negative sign). Mineral precipitation occurs according to transport-reaction eq. (2.4.4), and permeability and porosity reduction happen through the constitutive laws (2.4.6), (2.2.17), respectively. The bottom-hole pressure is monitored, and the simulation is halted when the pressure at the well-bottom remains less than 30% of the initial value of the well-bottom pressure.

$$p_{well} \leq 0.3\, p_{well,0}$$

The day that the simulation stops is considered as the exploitation lifetime of the well.

b) *Production with the inhibitor (PI):* This scenario consists of two cycles that are simulated periodically:

1) *Injection of the inhibitor:* Flow is inverted, and the inhibitor is injected in the domain with a predefined concentration for a fixed time. The (injecting) fluid is carrying a second species (inhibitor), entering through the well-screen (at a given rate of concentration), but not altering the fluid properties (density and viscosity). Mass transport equation for the inhibitor (2.4.5) is considered and the precipitation rate R_p is modified accordingly with eq. (2.2.22). In addition, the porosity decreases with eq. (2.2.23). Adsorption behavior of the inhibitor is modeled through the Langmuir isotherm. Within this cycle and the next one both the precipitating species and the inhibitor flow through the reservoir.

2) *Production:* When the injection process finishes, the well is set back on production. Inhibitor is present in the reservoir; the precipitation kinetics

is decreased thanks to the adsorption of inhibitor on the solid matrix. At the same time, the inhibitor continues to adsorb and can exit the domain through the well together with the production fluid. The maximum production period until the next injection is fixed to 1.5 year. However, injection is applied if the pressure at the bottom-hole attains a value less than 95% of the initial pressure of the present extraction (production) cycle:

$$p_{well} \leq 0.95\, p_{well,0}$$

We perform periodical injection-extraction (production) process until we reach the time which is the lifetime of the well that is obtained from the simulation of normal production. In this way we can compare the results of the two scenarios for the same amount of time.

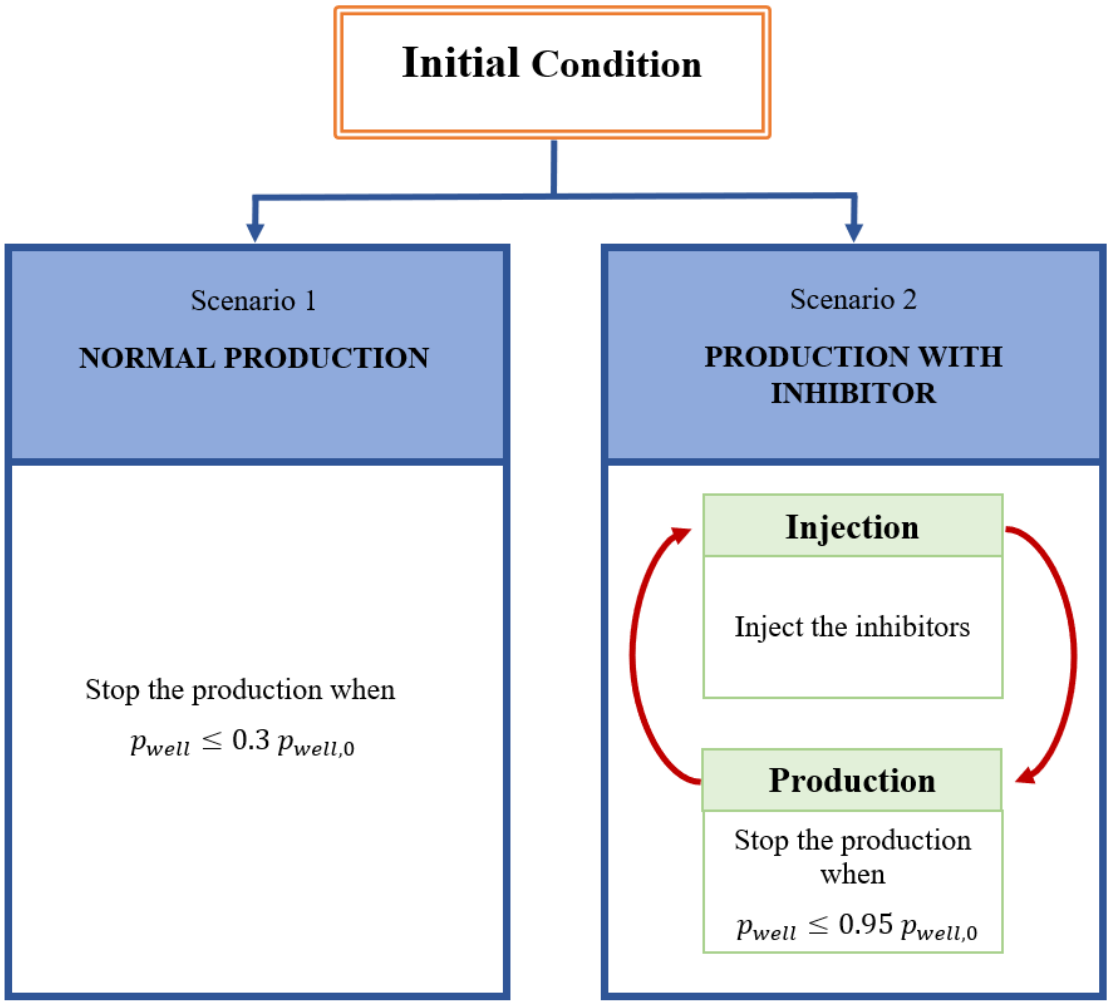

Figure 3.4.1: Simulation set-up

For normal production scenario, the model is simulated according to the following iterative procedure:

a) Find the initial condition (damage-free medium), according to the data given as input.
b) Select a time step (each time step represents a portion of the total simulation time, during which the input parameters are taken as constant)
c) For each time-step (Fig. 3.4.2):
    1) Use the velocity field from the previous step (or from the initial condition) to solve the transport-reaction eq. (2.4.4), to get the value of concentration of dissolved calcite at the present time.
    2) Use saturation index to calculate the precipitation rate of calcite using eq. (2.2.16).
    3) Calculate the porosity and permeability variation (2.2.17), (2.4.6).
    4) Use the new permeability to calculate the pressure (2.5.3) and the Darcy's flux (2.5.4) analytically.
    5) Update the variables, return to step 1) and repeat for the next step.

The above scheme is applied also to production with inhibitor scenario, with a slight difference; transport equation of inhibitor eq. (2.4.5) and Langmuir isotherm eq. (2.2.20) are included before 1) and the initial condition is substituted by the final solution of the previous cycle. Precipitation rate is calculated through eq. (2.2.22) considering the effect of the inhibitor. For the non-linear coefficient in front of the transient term in the inhibitor eq. (2.4.5), due to the non-linear adsorption isotherm, the solution of the previous time step is taken (explicit approach). Fig. 3.4.3 shows the simulation scheme for production with inhibitor, and Fig 3.4.4 shows the iterative procedure for each time-step of the injection and production cycles.

The output of the simulation consists in a set of variables i.e. pressure, calcite concentration, permeability, porosity, inhibitor concentration, precipitation rate. By comparing the variation of these variables during (and at the end of) the two processes, (namely, normal production and production with inhibitor) it is possible to make evident the beneficial application of the inhibitor to prevent the scaling by calcite precipitation in the reservoir.

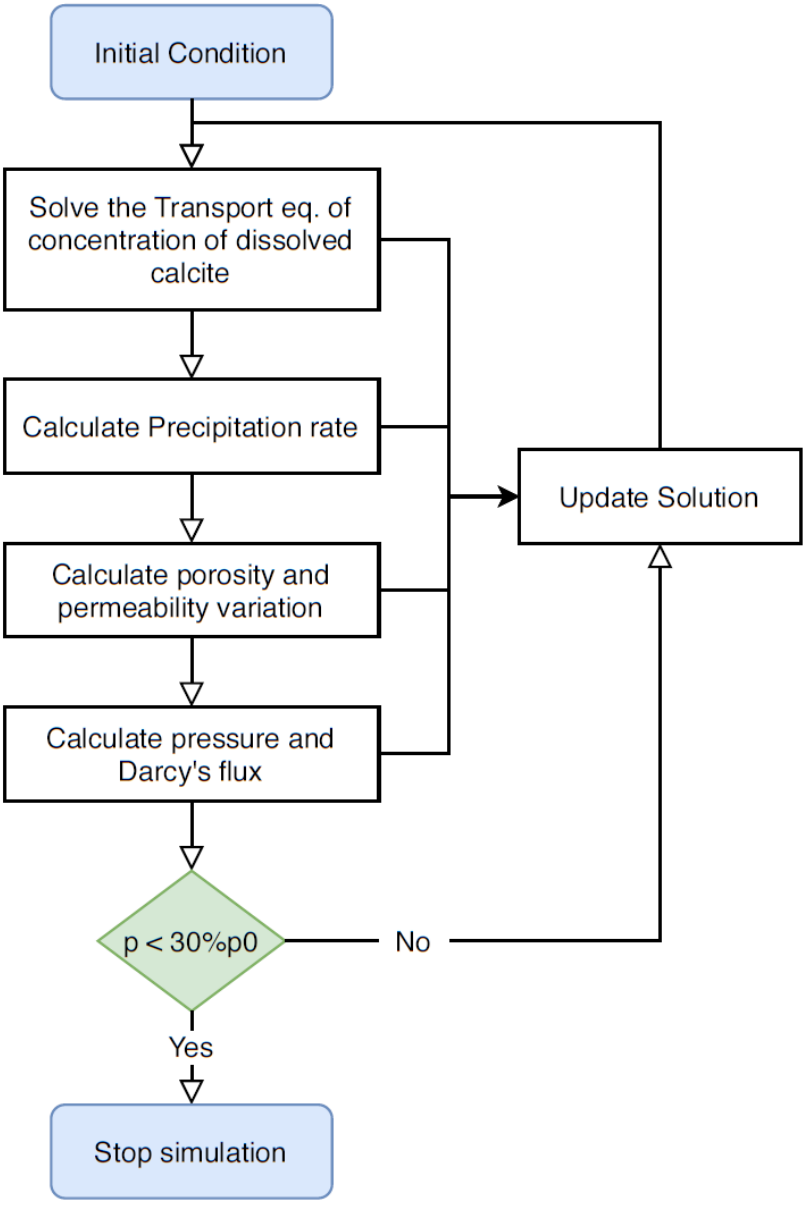

Figure 3.4.2: Normal production simulation scheme

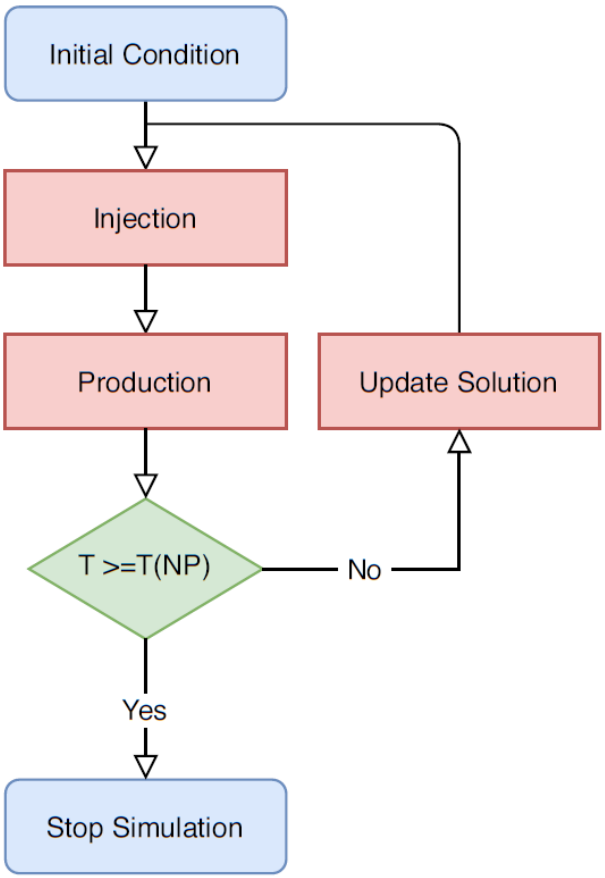

Figure 3.4.3: Production with inhibitor simulation scheme

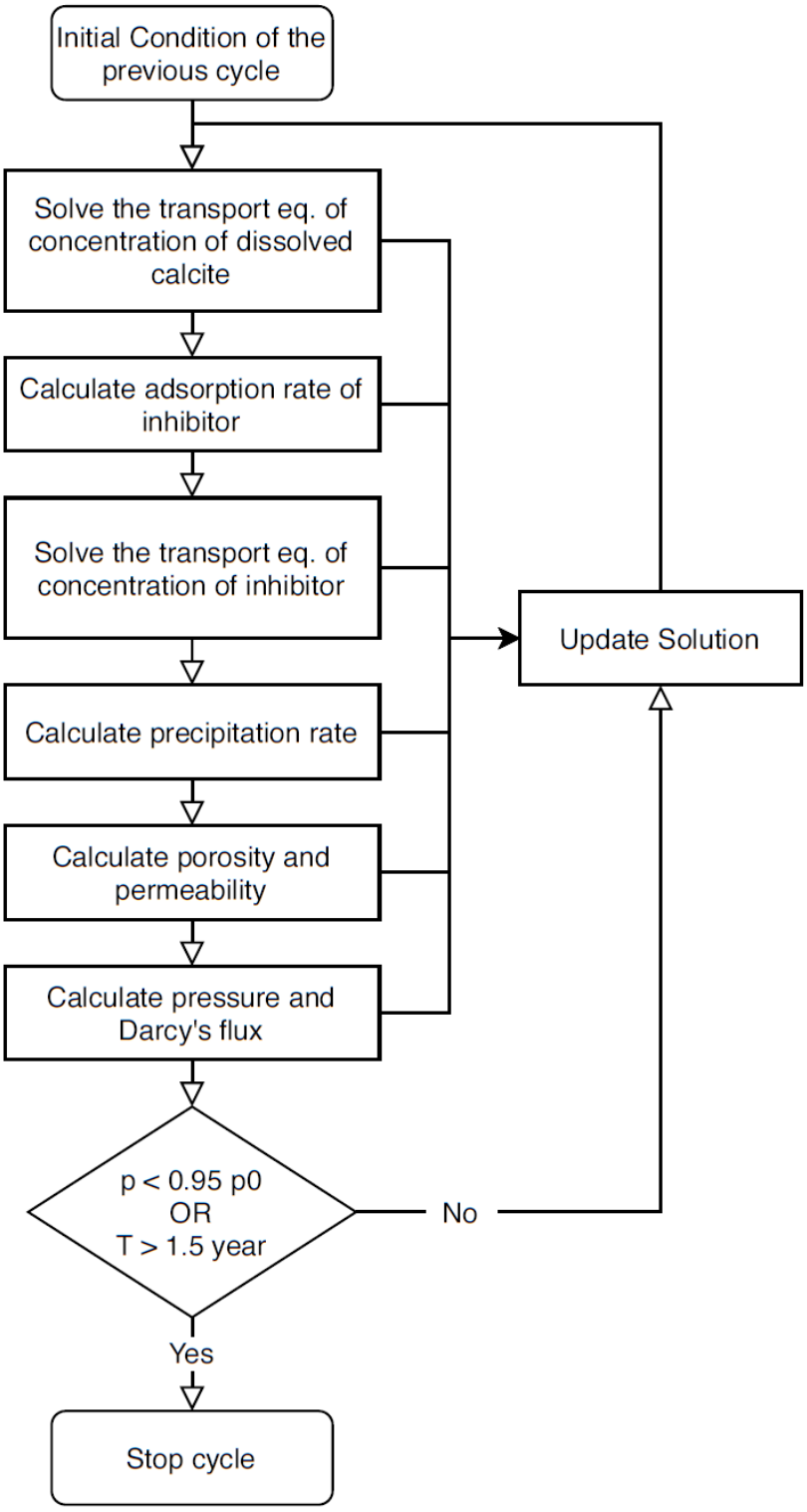

Figure 3.4.4: Iterative procedure for Injection/Production cycle

Chapter 4: NUMERICAL RESULTS AND ANALYSIS

In this chapter we analyse the results of the numerical simulations performed with the model developed in the previous chapters. First, we will see a reference case simulation followed by the analysis of mass conservation and convergence trends. Finally, we perform a sensitivity analysis by changing the key parameters of the precipitation and inhibitor to study the uncertainty of our model.

Parameters used in the simulation are obtained from the literature and the data provided from CHIMEC [9], and values for these parameters are found in Appendix.

4.1 Reference Case

For the reference case, the radial simulation domain (presented in section 3.1) is set as: $\Delta r_j = \alpha\, \Delta r_{j-1}$ (or $\Delta r_j = \alpha^{j-1}\, \Delta r_0$) where $\alpha = 1.05$ and $\Delta r_0 = 0.1$ m ($\Delta r_{max} \approx 23.6$ m). The length of the domain is $r_M = 500$ m with 115 nodes. The well radius is $r_w = 0.24$ m [9] and the height of the well screen is $H = 5$ m.

Production is simulated with time step $dt = 3$ hours (both for normal production and the production with inhibitor) and a fixed flow rate $Q = 100$ m^3/day [9] and through this value we are able to calculate the value of the Darcy's flux at the well:

$$u(r = r_w) = -\frac{Q}{2\pi r_w H} \cong -0.55 \text{ m/hour}$$

Here negative sign is due to the fact that fluid flows towards the well (during the injection process it is the opposite sign).

Boundary conditions for the pressure equation are defined as in equations (2.3.2) and (2.3.3) with $p_\infty = 231$ bars. In reality, the value of the pressure in the far boundary is typically unknown, this value for p_∞ is chosen to obtain $p_{0well} = 137$ bars as initial value of the pressure at the well-bottom as reported in [9].

The analytical solution of the steady-state pressure equation with the initial value of permeability $k_0 = 30$ mD and the Darcy's flux are taken as initial condition. From Fig. 4.1.1 we observe the steep increase in the pressure gradient near the well, which later gives rise to the steep increase in the absolute value of the Darcy flux close to the well in

Fig. 4.1.2. It should be mentioned that the production rate Q is fixed, so the Darcy flux at the well is constant and its magnitude decreases proportionally to 1/r.

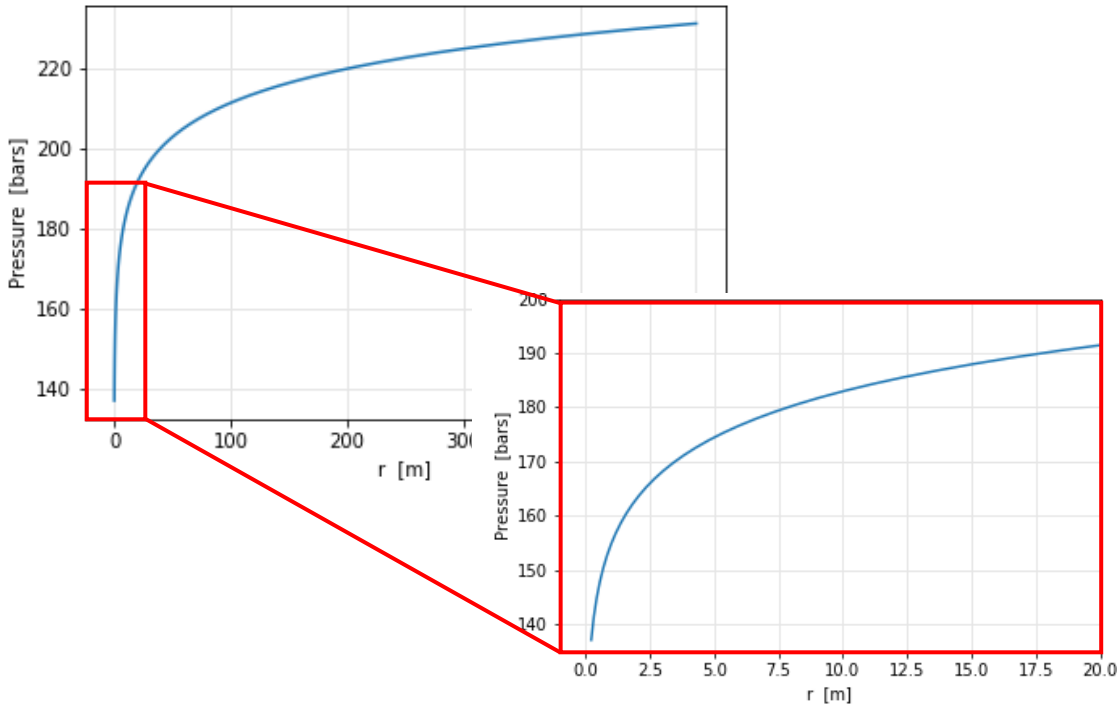

Figure 4.1.1: Initial pressure along the whole domain (above) and for r = [0, 20] m (below)

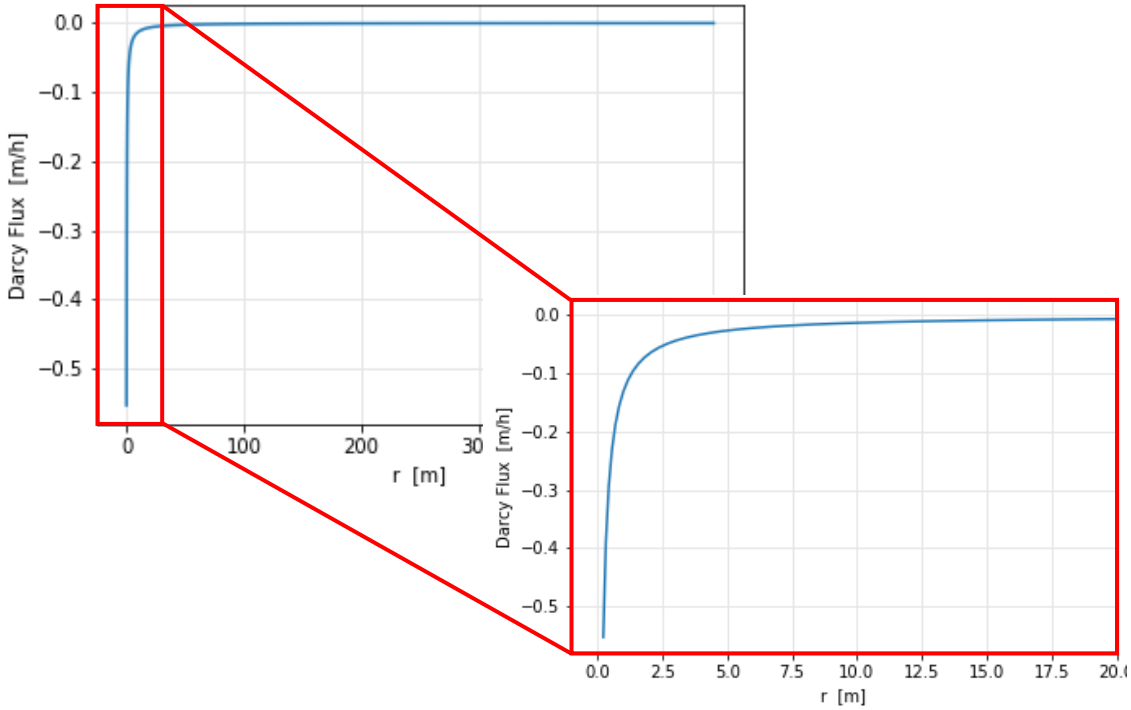

Figure 4.1.2: Initial Darcy's flux along the whole domain (above) and for r = [0, 20] m (below)

For the initial condition of the calcite concentration parabolic behaviour (demonstrated in eq. (2.3.8)) is chosen with the saturation index (SI) $\Lambda_i = 30$ at the well-bottom (which is the lowest measured value of SI of calcite reported in [9]) and it is depicted in Fig. 4.1.3. Note that in reality it is typically not possible to determine the SI of a specific mineral on the whole domain. In practice, SI can be measured at the well-bottom (or creating the well-bottom conditions in a laboratory environment). The reason to impose a parabolic initial condition is to satisfy the zero-Neumann boundary condition at the well (imposed in eq. 2.3.5) during the production phase and a smooth decay of the concentration over the domain. Equilibrium Dirichlet boundary condition (eq. 2.3.7) is appointed on $r = R$, namely, $SI = 1$ on the far boundary.

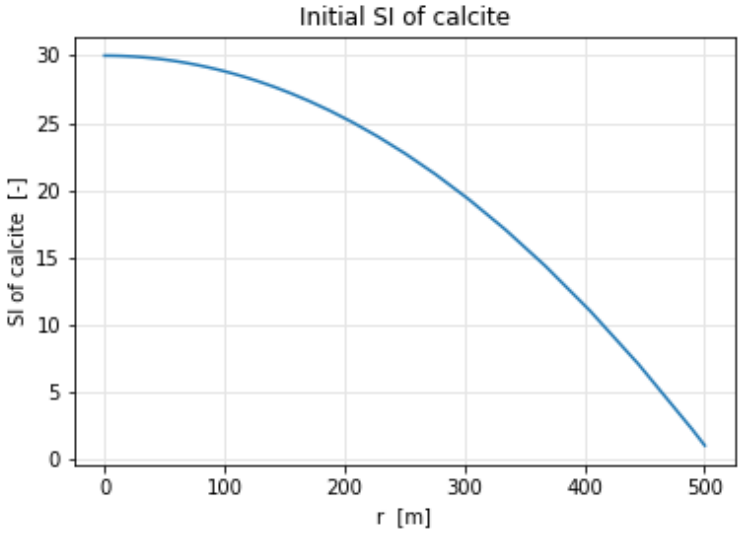

Figure 4.1.3: Initial condition for the calcite concentration

The inhibitor used for the reference case is a product of CHIMEC S.p.A and the adsorption-desorption of the inhibitor is modelled with Langmuir isotherm (eq. 2.2.20) as recommended in [9].

$$F = F_{max} \frac{b\, c_i}{1 + b\, c_i}$$

where adsorption energy coefficient $b = 73\ 10^{-3}$ l/mg and maximum adsorption capacity $F_{max} = 1.28$ mg/g. Values of these parameters are obtained through the laboratory experiments reported in [9].

As a reference case, inhibitor is injected from the well screen to the domain at flow rate $Q = 100$ m^3/day with a concentration of 35 g/l for 0.4 day [9], and time step $dt = 60$ sec. Hence, we impose a constant Dirichlet boundary condition at the well equal to 35 g/l during the injection phase. During the production phase zero-Neumann boundary condition is applied as it was done for the transport-reaction equation of calcite concentration. On $r = R$ homogenous Dirichlet boundary condition is applied through the whole simulation.

Fig. 4.1.4 (left) shows the inhibitor concentration profile around the well after the injection phase. We observe that the inhibitor tends to zero for to $r > 3$ m. This result shows that the inhibitor treatment will be effective 3 m around the well, according to our simulation results.

Fig. 4.1.4 (right) depicts the results obtained from a simulation (with the same flow rate, inhibitor injection concentration and injection time) which is performed with SARIP^{CH} that is a commercial reservoir simulator [9].

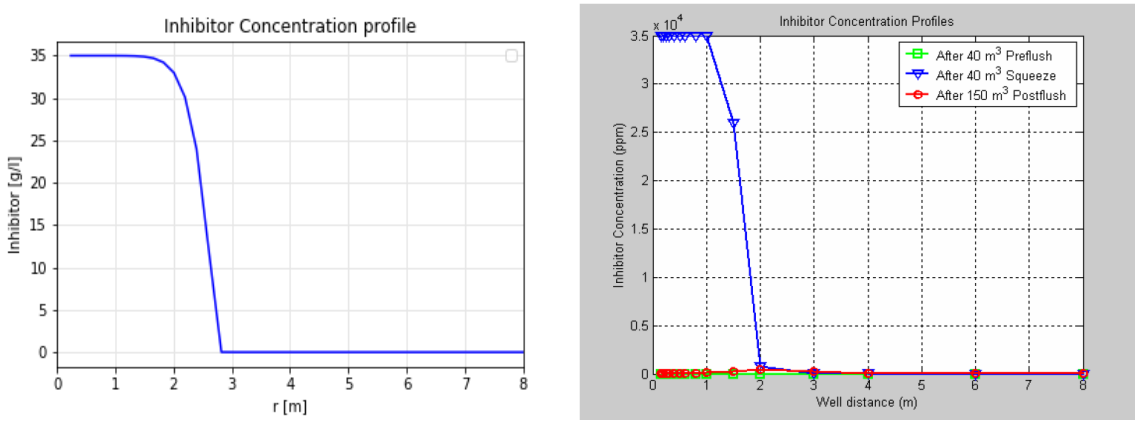

Figure 4.1.4: Inhibitor concentration around the well after the injection. Left: Simulation performed with the model developed in this thesis. Right: Simulation performed with SARIP^{CH} (ref: [9]).

Both simulations are performed with the same parameters for the inhibitor and the reservoir properties (porosity, permeability, well radius). The difference between the two simulations is that SARIP^{CH} simulation is done on a two-dimensional (r, z) domain assuming the angular symmetry of the reservoir, instead our model is on a one-dimensional radial domain. Also, SARIP^{CH} simulation is designed with three phases: preflush, injection, postflush. In the preflush and postflush phases, the reservoir is washed using a fluid that is the same one in which the inhibitor is solved during the injection phase. We do not perform these two phases. Moreover, we do not have any information about some of the important reservoir properties, such as dispersivity and the bulk density of the porous medium. In spite of minor differences, we observe that the result of our simulation is consistent with the result of SARIP^{CH} simulation.

In figure 4.1.5 we can see the inhibitor adsorption profiles obtained from Langmuir isotherm. We observe that the dissolved inhibitor is stored on the rock surface by adsorption over the 3 m around the well.

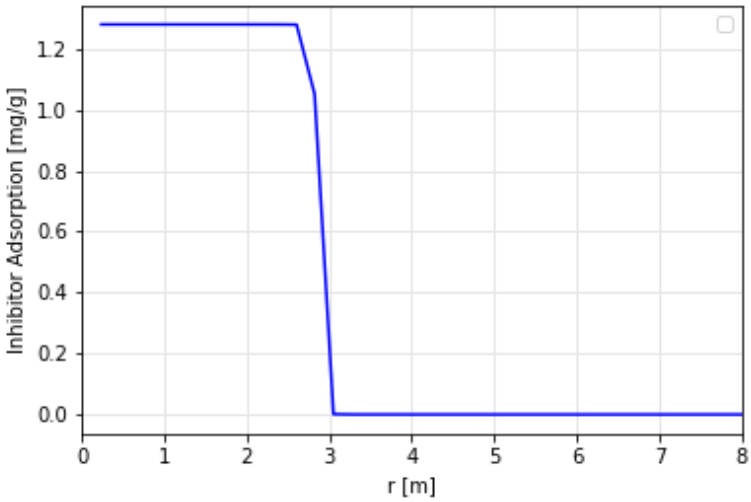

Figure 4.1.5: Inhibitor Adsorption profile after the injection

In the following graphs we observe how pressure, saturation index of calcite concentration, inhibitor concentration, permeability, precipitation rate and porosity changes over time and in the near-well zone of the domain. We will compare the results of the normal production and production with inhibitor and present the efficiency of the inhibitor treatment.

(in the following: NP = Normal Production, PI = Production with Inhibitor, IC = Inhibitor Concentration)

Fig. 4.1.6 shows the inhibitor concentration at the well versus time, in linear and semi log scale. We observe a sharp decrease of IC right after starting the extraction from which we can understand that the remaining mobile (not adsorbed) inhibitor leaves the domain in a short time after starting the production cycle.

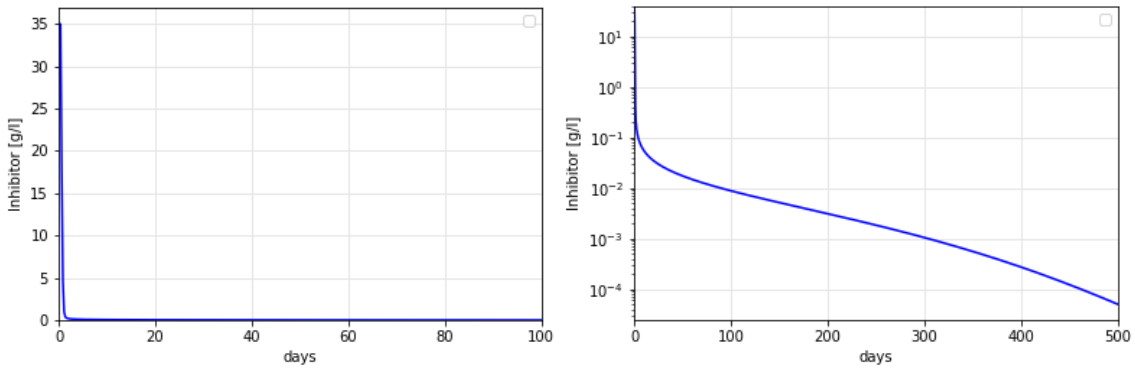

Figure 4.1.6: Inhibitor concentration at the well vs time in linear (left) and semi log (right) scale

Fig. 4.1.7 depicts the evolution of the pressure at the production well for both NP and PI. As noted, the initial value of the pressure at the well-bottom p_{0well} is 137 bars.

Normal production is simulated until this value remains less than 30% (as reported in section 3.4). NP simulation stops on day 3522 (slightly less than 10 years) with well-bottom pressure equal to 41 bars. This value as an exploitation time of a well is considered as natural lifetime of a geothermal production well.

During the PI simulation, injection of the inhibitor is repeated periodically. Maximum PI period until the next injection is fixed to 1.5 year, but if the pressure at the well reaches a value equal to the 95% of the initial well-bottom pressure of the current PI phase, next injection is performed before reaching 1.5 years (section 3.4). This periodical injection-production process is simulated until we reach the day 3522 which is the time obtained from NP simulation. In this way we can compare the well pressure of NP and PI for the same day. Pressure at the well in PI simulation on day 3522 is 92 bars. This value is more than double from what we obtained from NP simulation (41 bars). This difference between the two pressures affects the operational cost; when the well pressure is low there is the need to install larger pumps or the operation time extends. During PI simulation (3522 days) inhibitor is injected 8 times. This is an important factor in the inhibitor injection treatment design. In practice, the biggest impediment to periodic injection-production process is to remove the pump, set up the injection devices and put back the pump to its place for the next extraction (production) phase. Depending on the type of the well and the reservoir this procedure sometimes can be very time-consuming and costly. Therefore, the well details, reservoir conditions and the injection parameters should be studied carefully before applying the treatment.

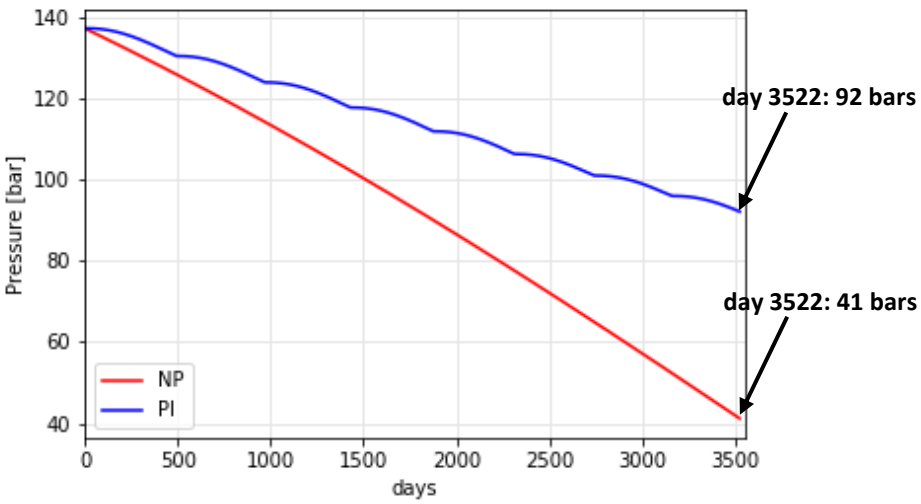

Figure 4.1.7: Pressure at the well during the NP and PI

Fig. 4.1.8 shows the pressure profiles in the near-well zone of the domain (3.5 m around the well). We can clearly see the inhibitor is more effective (described by double-headed arrows on Fig. 4.1.8) very close to the well than faraway and this can be explained by the fact that inhibitor adsorption rate (Fi. 4.1.5) is higher close to the well (because of the high value of the concentration of the inhibitor (Fig. 4.1.4)). In fact, the two pressure profiles of NP and PI collapse right after the influence area of the inhibitor ($r \approx 3$ m).

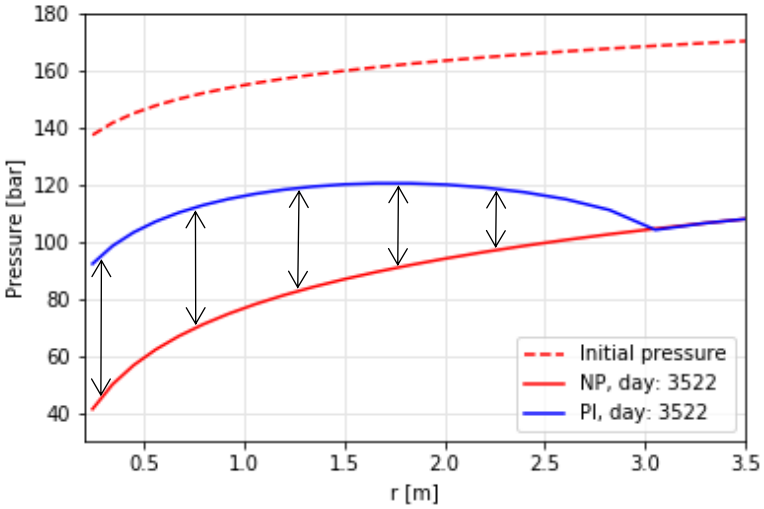

Figure 4.1.8: Pressure decrease after NP and PI at the near-well zone

Fig 4.1.9 (left) and (right) shows the permeability and the porosity decrease at the well-bottom for NP and PI simulations, respectively. A special attention should be paid to the fact that permeability is predicted to decrease by more than 50% in NP, while porosity decrease by less than 18%. This is due to the fact that in our model permeability depends on porosity exponentially (eq. 2.2.19). The reason to choose this kind of model is that the pore throat clogging can cause more permeability damage than solid surface deposition [1]. Hence, the permeability reduction is represented by an exponential decay with the effective fractional bulk volume ε_p. After PI simulation permeability damage at the well is measured as 33%, while porosity decrease is only 9.7%.

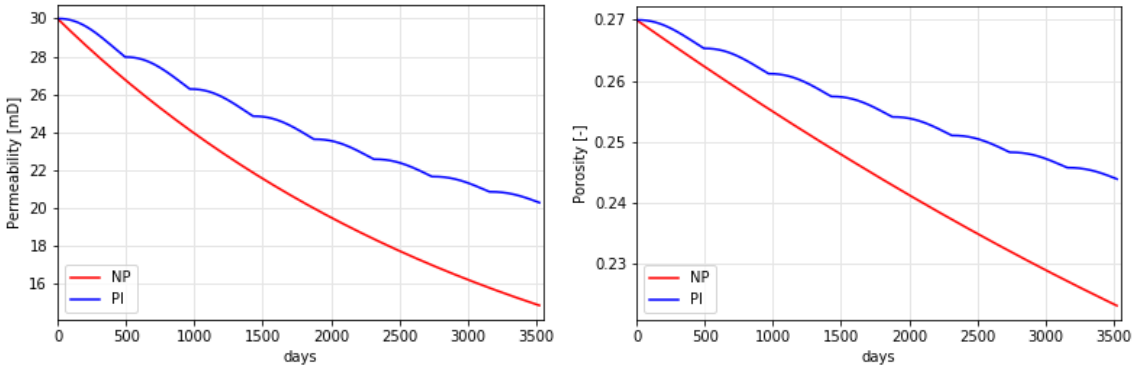

Figure 4.1.9: Permeability (left) and porosity (right) decrease at the well-bottom during NP and PI

Fig 4.1.10 (left) and (right) shows the permeability and the porosity profiles at the near-well region for NP and for different time steps of PI. We observe the same behavior as we did for pressure profile; results of NP and PI simulations collapse at $r \approx 3$ m.

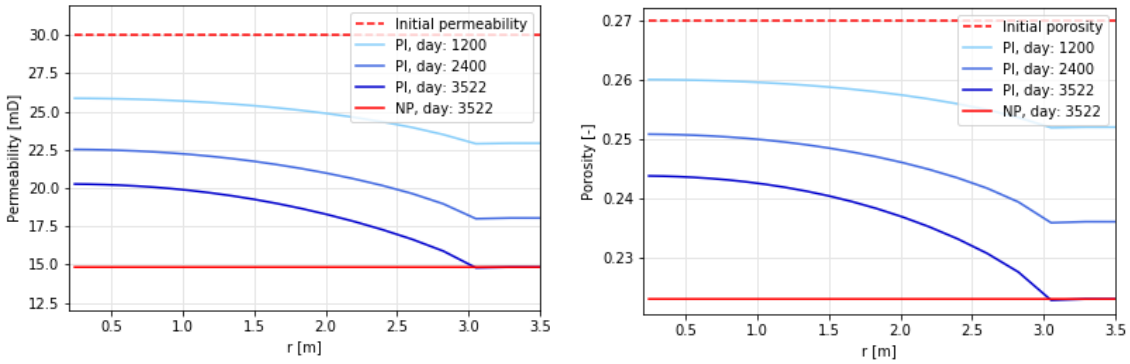

Figure 4.1.10: Permeability (left) and porosity (right) profiles in the near-well region for different time steps.

Fig. 4.1.11 shows the first two cycles of injection-extraction process. We see that right after the injection of the inhibitor, the precipitation rate (eq. 2.2.16) decreases approximately four orders of magnitude, showing the effect of the inhibitor (eq. 2.2.22). With production the concentration of the inhibitor in the reservoir decreases since part of it is extracted with the production fluid. Obviously, as a consequence the precipitation rate increases gradually. It is important to note that, in literature, it is generally assumed that the inhibitors do not change the solubility of the precipitating component, but they modify the kinetics of the crystallisation only. More precisely, the inhibitor prevents the precipitation by adsorbing on the solid surface itself. After the second injection the precipitation trend repeats itself and it continues in the same way for the following cycles.

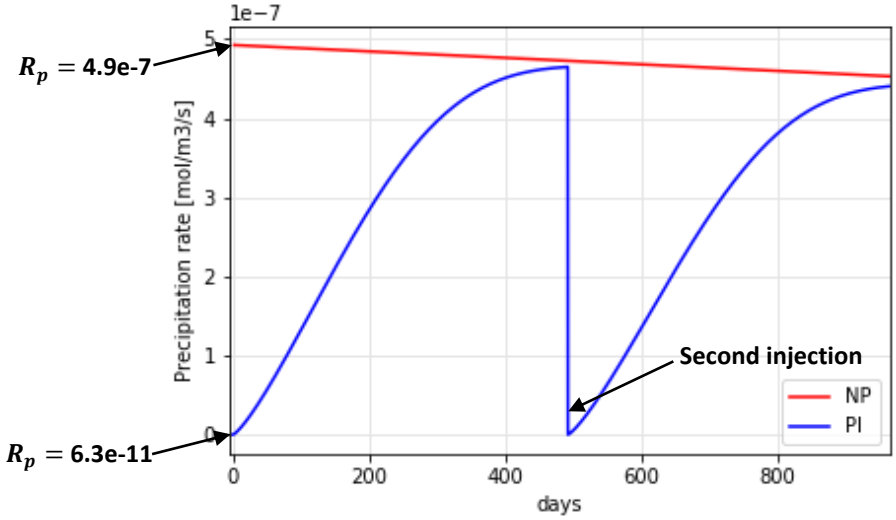

Figure 4.1.11: Precipitation rate of calcite at the well during NP and PI

Fig. 4.1.12 portrays the saturation index (SI) of calcite concentration at the well during NP and PI simulation. We observe a decrease of SI with time in both simulations. This result is justified upon observing that, as previously mentioned, dissolution from the rock surface is not considered in our model. Hence, SI decreases (until it can reach the equilibrium concentration) as a result of precipitation. Moreover, since we imposed zero-Neumann boundary condition at the well during the production phase (eq. 2.3.5), some of the dissolved calcite (corresponding to the dissolved ions) is extracted from the domain. In a real case situation, this observed decay of dissolved minerals might display a milder slope because dissolution is present.

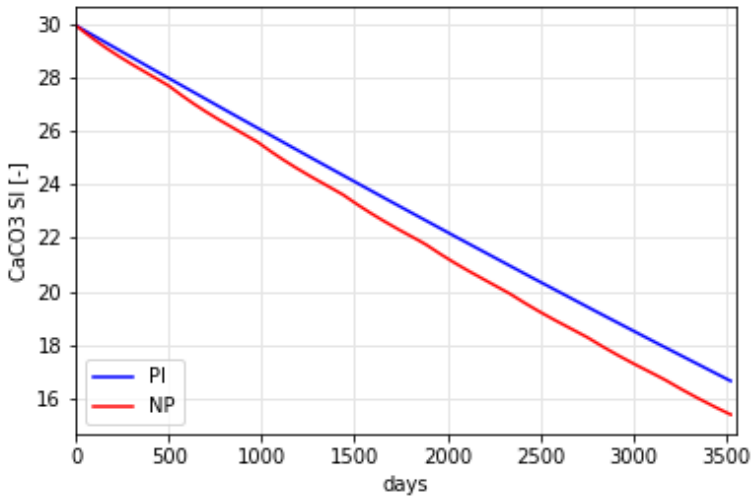

Figure 4.1.12: Saturation index of calcite concentration at the well during NP and PI

4.2 Code verification

Code verification is a process to ensure that there are no errors (bugs) in a computer code or inconsistencies in the solution algorithm. In this thesis, we study the mass balance and convergence trends of the model, and also report the computational times of the code.

Mass balance. Mass balance (conservation of mass) is a physical law which states that a matter inside the system cannot disappear or be created spontaneously. Failure of the mass conservation law within an acceptable tolerance is an indication of a mistake in the numerical model. For our model we check the mass balance for the injected inhibitor, as the inhibitor injection phase is the most computationally demanding phase of the simulation, because it entails both the nonlinear precipitation and adsorption processes.

For the reference scenario the inhibitor is injected to the domain at flow rate $Q =$ 100 m^3/day with concentration $c =$35 kg/m^3 for injection time $T_i = 0.4$ day. Hence, the total injected mass of the inhibitor is:

$M_{injected} = Q\ c\ T_i = 1400$ kg

Injection is simulated with time step $dt = 60$ sec. A part of the inhibitor remains mobile in the domain (depicted in Fig. 4.1.4 (left)), and the rest adsorbs to the solid matrix with the rate defined by the Langmuir adsorption isotherm eq. (2.2.20) (Fig. 4.1.5). The mass of the mobile inhibitor and mass of the adsorbed inhibitor are calculated with the following formulae (considering the cylindrical shape of the domain):

$$M_{mobile} = \pi H \sum_{j=0}^{M-1} \left(r_{j+1}^2 - r_j^2\right) \frac{\left(c_j + c_{j+1}\right)}{2} \frac{\left(\phi_j + \phi_{j+1}\right)}{2} \qquad 4.2.1$$

$$M_{adsorbed} = \rho_b \pi H \sum_{j=0}^{M-1} \left(r_{j+1}^2 - r_j^2\right) \frac{\left(F_j + F_{j+1}\right)}{2} \qquad 4.2.2$$

where H [m] is the height of the screen.

The total mass in the domain is the sum of the mobile and the adsorbed parts of the inhibitor:

$$M_{total} = M_{mobile} + M_{adsorbed} \qquad 4.2.3$$

Mobile mass in the domain after the injection phase is calculated through the eq. (4.2.1) and the result is $M_{mobile} = 939.65$ kg. The result for the adsorbed mass calculated with the eq. (4.2.2) is $M_{adsorbed} = 420.45$ kg. Hence, the total mass inside the domain is $M_{total} = 1360.1$ kg. Then the discretization error with respect to the actual injected amount of inhibitor (1400 kg) is 2.85%. Fig. 4.2.1 shows the amount of the injected inhibitor in the domain (left) and the discretization error (right) versus injection time.

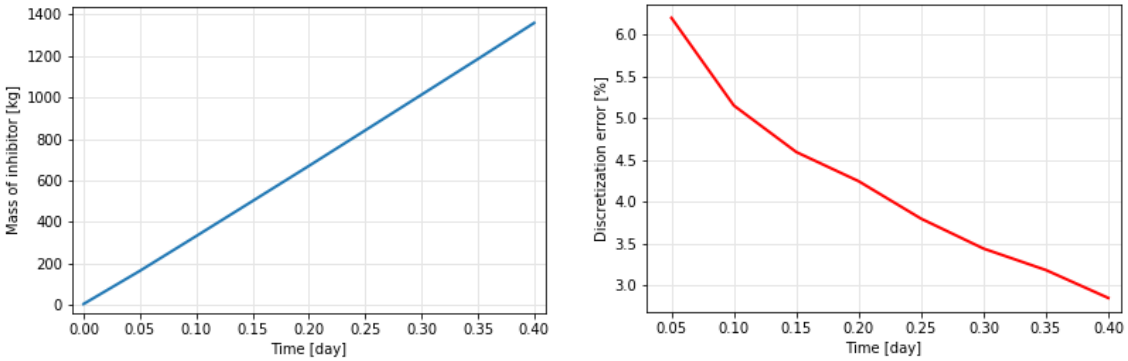

Figure 4.2.1: Mass of inhibitor and the mass balance error as a function of time

The numerical error on material balance is induced by the approximation method selected. We have verified that the numerical mass balance error can be controlled by reducing the space and time discretization. Indeed, in Fig 4.2.2 we observe that using smaller (uniform) grid size and time step size decreases the discretization error.

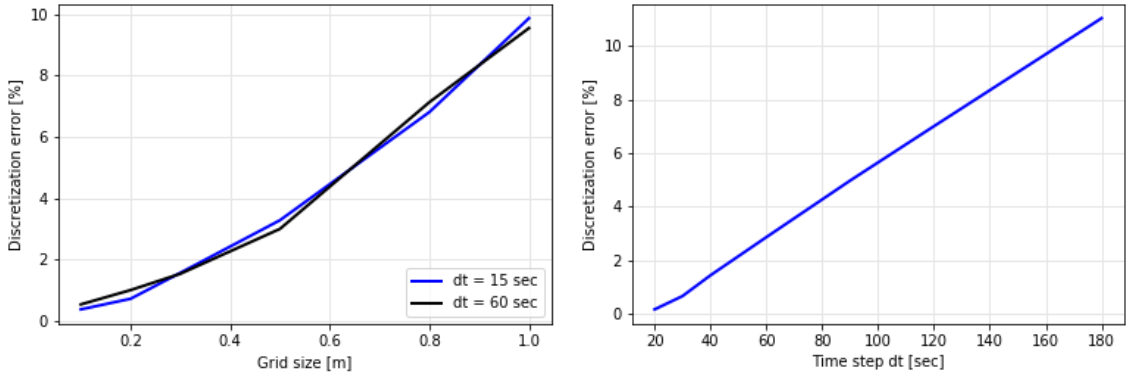

Figure 4.2.2: Mass balance error versus uniform grid size dr (left) and versus time step dt with fixed non-uniform domain with 115 grid points (right)

Convergence analysis. GCI method described in section 3.3 is employed to analyse the convergence trends. Normal production and injection phase are simulated with three different uniform grid sizes. In particular, we focused on the pressure after the normal production phase and on the inhibitor profile after the injection phase.

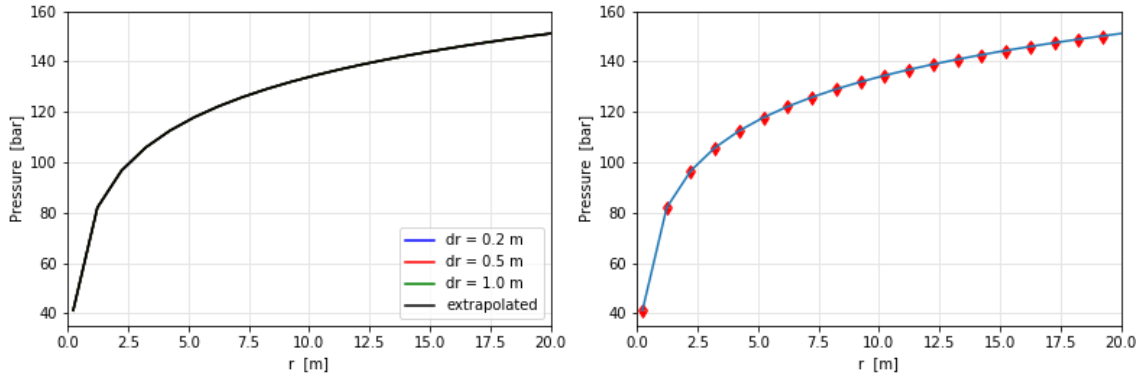

Figure 4.2.3: (left) Pressure profiles computed with three grid size and extrapolated values; (right) Fine-grid solution with discretization error bars computed using eq. (3.3.5)

Fig. 4.2.3 (left) presents the pressure profiles after the normal production simulated with three different uniform grid sizes $\Delta r_1 = 0.1$ m, $\Delta r_2 = 0.5$ m, $\Delta r_1 = 1.0$ m. The order of accuracy q is calculated through eq. (3.3.2) ranges between 0.35 and 6.53 with a global average $q_{ave} = 1.12$. The values of order of accuracy are used to assess the GCI index values in eq. (3.3.5) for individual grids, which is plotted in the form of error bars, as shown in Fig. 4.2.3 (right). No oscillatory behaviour is observed, and the maximum discretization uncertainty is $4.66 \cdot 10^{-7}$ % which is observed at the well $r = r_{well}$.

GCI analysis for the inhibitor concentration is performed only in the first 6 m of the domain, since as it was noted in section 3.3 that when the difference between any two simulations or the output values themselves are very close to zero, GCI analysis is not valid. Figure 4.2.4 (left) shows the inhibitor profiles after the injection phase with uniform grid sizes $\Delta r_1 = 0.1$ m, $\Delta r_2 = 0.15$ m, $\Delta r_1 = 0.3$ m. The order of accuracy q ranges from 0.42 to 15.32 with a global average $q_{ave} = 3.10$. Oscillatory convergence is observed only in one point which is 0.3 m away from the well. Discretization error bars are shown

in Fig. 4.2.4 (right), along with the fine-grid solution. The maximum estimated relative discretization error is 0.15 %.

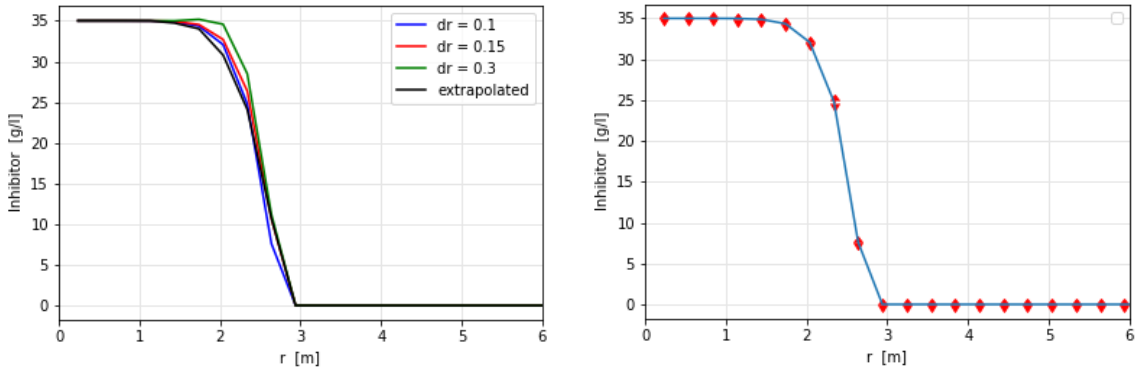

Figure 4.2.4: (left) Inhibitor profiles computed with three grid size and extrapolated values; (right) Fine-grid solution with discretization error bars computed using eq. (3.3.5)

Computational efficiency of the code. Computational efficiency measures the amount of time required for a numerical calculation. Fig. 4.2.5 (left) and Fig. 4.2.5 (right) show the computational time with respect to the number of nodes (with fixed time-step size $dt = 3$ hours) and with respect to the time-step size (with fixed number of nodes $M = 115$) in log-log scale, respectively, simulated with HP Pavilion with Intel(R) Core(TM) i7-8565U CPU @ 1.80 GHz and 16 Gb RAM.

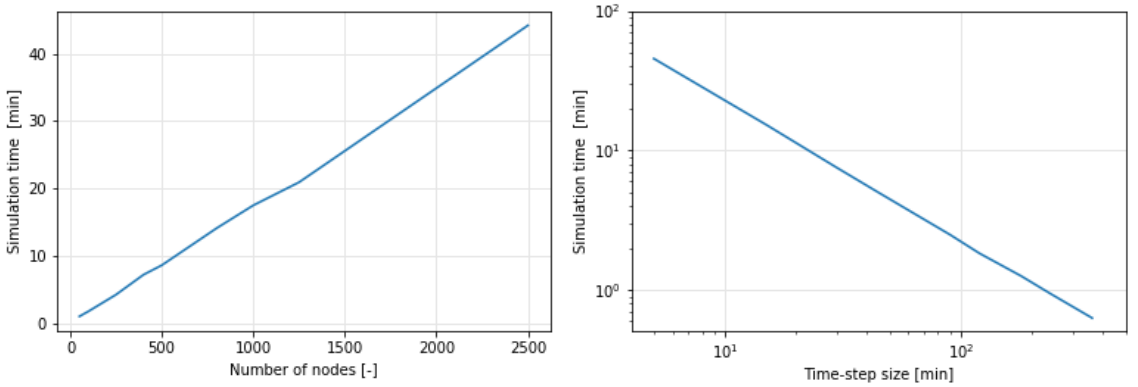

Figure 4.2.5: Computational time versus the number of nodes with fixed dt=3 hours (left) and versus time-step size with fixed M=115 with log-log scale(right)

4.3 Sensitivity analysis

To study the effect of the inputs uncertainty on the output of our model sensitivity analysis is performed. For the sensitivity analysis we consider as a key output the value of pressure at the well. We have performed sensitivity analysis for NP and PI simulations separately.

For NP our aim is to analyse the effect of the initial value of saturation index SI at the well (again with parabolic behaviour over the rest of the domain) and the reaction rate k_p of the concentration of dissolved calcite. These two parameters are the key factors of the mineral precipitation process, and are strongly dependent on reservoir field conditions (e.g. temperature, pH) which are often challenging to characterize. By changing these two parameters in a chosen interval we will study how the well pressure decrease over time as a function of the kinetics of the reaction process. NP sensitivity analysis is performed with the same stopping condition, namely, the simulation stops when well pressure reaches less than 30% of the initial well pressure. In this case, we compare the well exploitation lifetime for different values of SI and k_p.

Fig. 4.3.1 shows the well exploitation times as colour map which is the result of 400 simulations. SI changes over the interval [15, 110] and k_p is in [5e-11, 5e-10]. With the smallest values of SI and k_p exploitation time can reach a value over 7300 days (20 years). The highest values of SI and k_p yield to a well exploitation time of 314 days (less than one year).

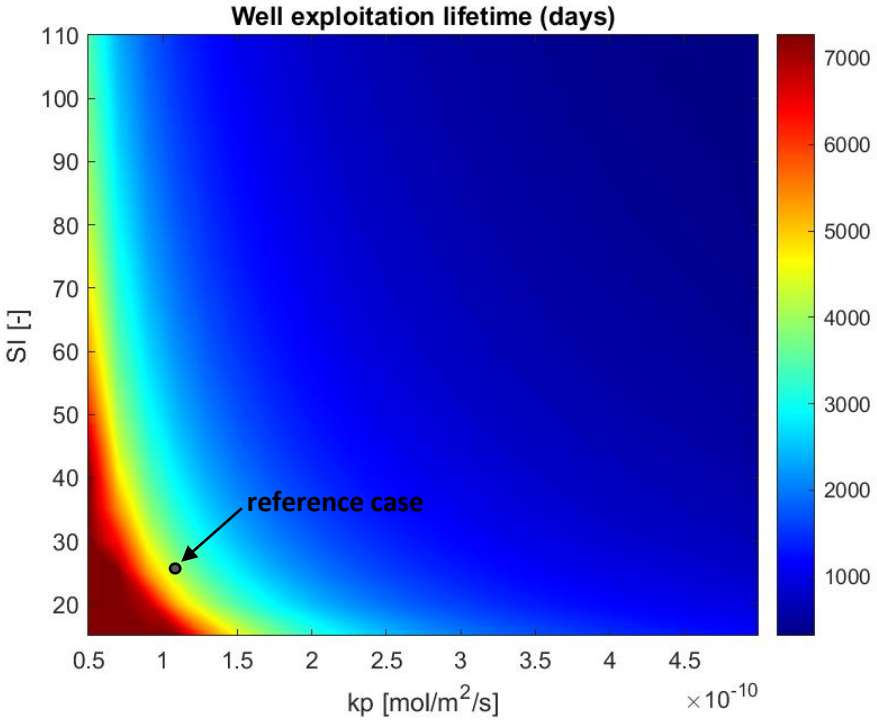

Figure 4.3.1: Colour map of well exploitation lifetime in days

In order to quantify the importance of the parameters (inputs) on the variance of the output (well exploitation lifetime) we use the Sobol sensitivity indices following the procedure described in [25]. We found the following Sobol indices:

$S_{SI} = 0.206$

$S_{kp} = 0.667$

which indicates that the reaction rate k_p has a bigger effect on the process than the saturation index SI. Fig. 4.3.2 shows the conditional averages of the exploitation time versus SI and k_p. The well exploitation time decreases as both parameters increase. Consistent with the reported Sobol indices values, we observe that the reaction rate k_p induces a larger variation of exploitation time as compared to the initial SI within the investigated parameter space.

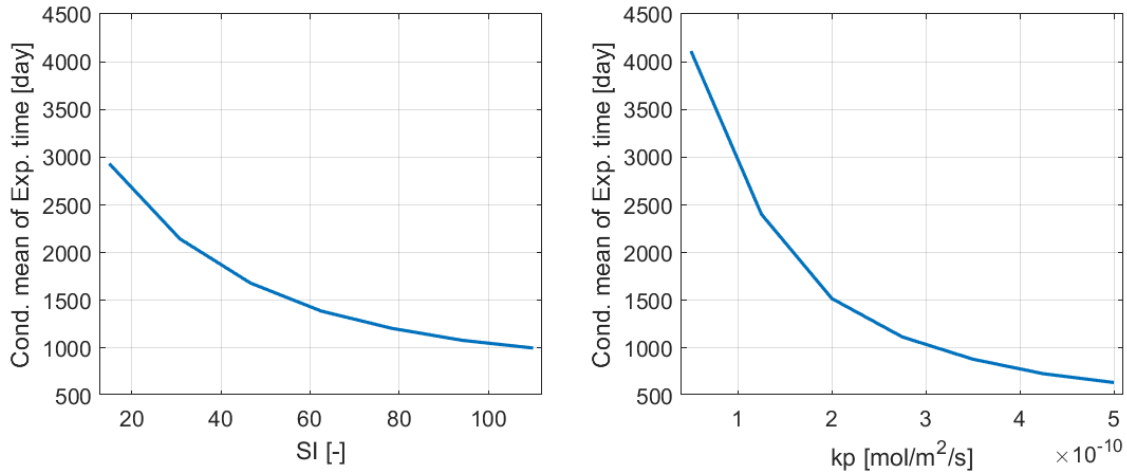

Figure 4.3.2: Conditional averages of exploitation time vs SI (left) and kp (right)

For the sensitivity analysis of PI simulation, we study the inhibitor properties, namely, maximum adsorption capacity F_{max}, inhibitor injection concentration c_i and the injection time T_i. By way of this analysis we compare the effects of the treatment design (concentration and injection time) against the chemical characterization of the inhibitor (maximum adsorption capacity). Saturation index and reaction rate remain as in the reference case (section 4.1). We study the value of the well pressure at time = 3522 days which is the time obtained from the NP simulation of the reference case (section 4.1). In this way we can study the possible inhibitor treatment scenarios for the reference case.

In total we have done 8000 simulations and the interval ranges for the input parameters are as follows:

$F_{max} \in [0.64, 3.072]$ mg/g

$c_i \in [10, 48]$ g/l

$T_i \in [0.1, 2.0]$ day

We obtained the following Sobol indices:

$S_{F_{max}} = 0.0623$

$S_{ci} = 0.0528$

$S_{T_i} = 0.8223$

Injection time T_i is clearly dominating over the other two parameters which is actually expected.

Fig 4.3.3 shows the probability distribution function (pdf) histogram of the well pressure obtained by sampling the considered parameter space. As a result of the assumed parameter variability we obtain values of pressure changing between 50 and 130 bars, with a left tail towards lower values. Because lower values indicate a loss of performance of the treatment it is important to understand which parameter drives the occurrence of such low values.

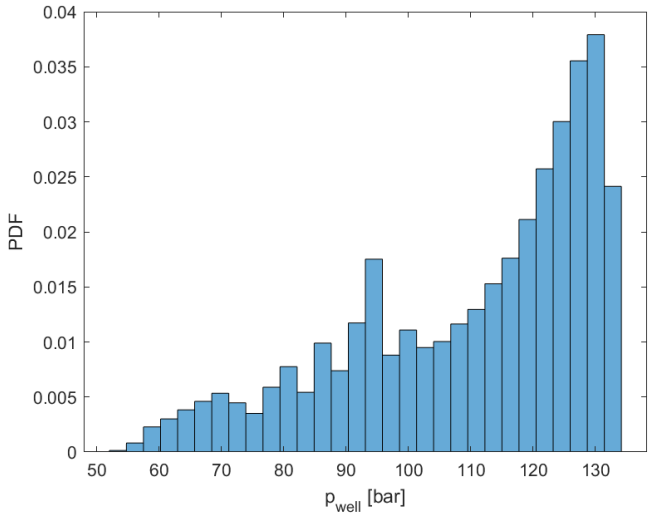

Figure 4.3.3: PDF histogram of the well pressure

To understand the impact of the parameters on the predicted pressure values we consider conditional statistics. In Fig. 4.3.4 and Fig. 4.3.5 we observe the output and the conditional averages of the well pressure with respect to F_{max}, c_i and T_i, respectively. We see that the pressure exhibits a clear increasing trend with the injection time while is only mildly sensitive to the other parameters. In particular, critically low values of pressure (e.g., p_{well} < 90 bars) are all associated with an injection time smaller than 1 day. Moreover, the analysis suggests that the inhibitor concentration is not a critical parameter in designing the treatment. At the same time, the uncertainty on the affinity between the inhibitor and the reservoir rock is expected to play a relatively minor role, at least under the considered assumptions.

The above discussion is consistent with the values assumed by the Sobol indices.

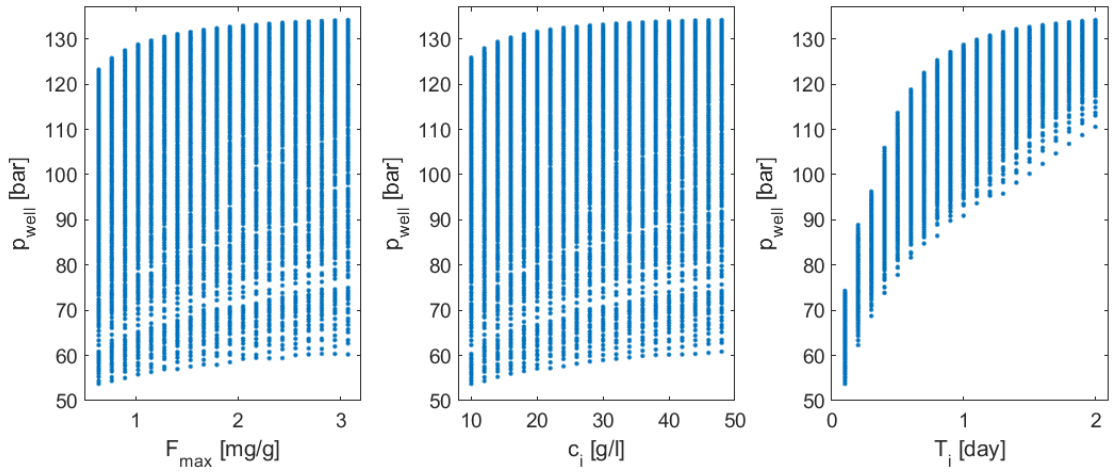

Figure 4.3.4: Well pressure profiles versus Fmax (left), ci (middle) and Ti (right)

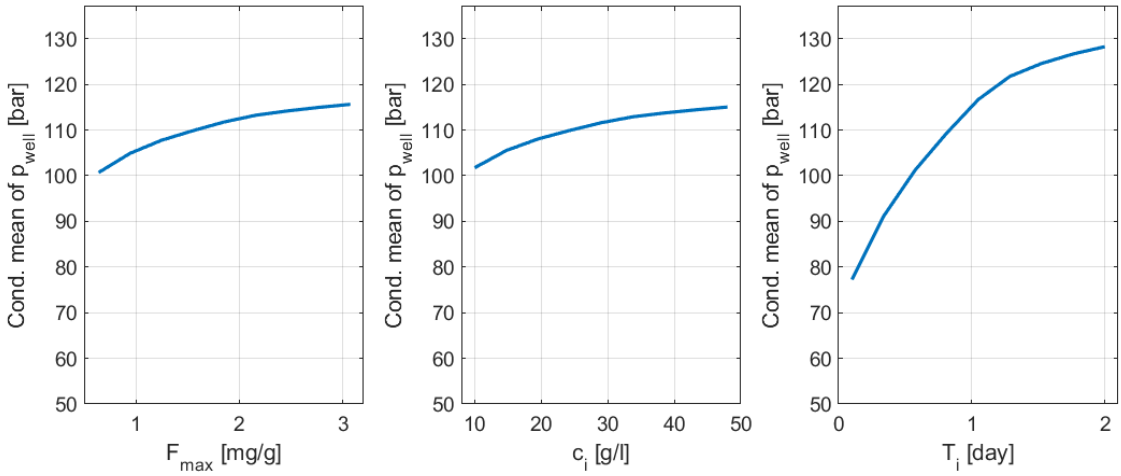

Figure 4.3.5: Conditional averages of the well pressure versus Fmax (left), ci (middle) and Ti (right)

Chapter 5: CONCLUSIONS AND FUTURE DEVELOPMENTS

This thesis considers the problem of formation damage in subsurface reservoirs in the near-well region by mineral precipitation and develops a numerical simulation tool to control and quantify the effects of the injection of specific chemical substances to control this issue. These chemical substances are called inhibitors and hamper the precipitation process by influencing its kinetics without having any effect on the solubility of the precipitating matter.

In this thesis a novel numerical simulation tool has been implemented and numerically verified. This tool can be used as a profiling tool to analyse the performance of inhibitors in the reservoirs. The simulation setting is simplified, but the code is already able to provide practically useful information about the process. In particular, we consider literature formulations to build a mathematical model which consists of system of PDEs and constitutive laws to model the following processes:

- Single phase fluid flow in a radial domain,
- Solute transport in the presence of precipitation-dissolution,
- Solute transport of the injected inhibitors,
- Porosity and permeability reduction as a result of precipitation.

Considering a single-well model, a number of assumptions are made on the porous medium and the fluid properties. The corresponding numerical simulation tool is implemented in Python environment using the finite difference method on a non-uniform one-dimensional radial grid.

The numerical model is employed in this work to simulate two scenarios, namely, normal production and production with the inhibitor. During normal production the simulation stops when the pressure at the well-bottom decreases by 70% with respect to its initial value. In the production with inhibitor scenario a fluid with the dissolved inhibitor is injected from the well into the reservoir. The design parameters of the process are the inhibitor concentration and the injection time period. After an injection cycle the well is set back to production with the inhibitor being present in the reservoir. In this scenario, injection and production phases happen periodically until a prescribed time is reached. At the end of the simulation normal production and production with inhibitor results are compared to quantify the effects of the inhibitor in preserving the reservoir permeability in the near-well region.

Various scenarios with different saturation index and reaction rate of precipitating species, inhibitor concentration, injection time and inhibitor chemical properties are

simulated numerically within a sensitivity analysis study to analyse in detail the response of the system.

In the considered numerical test, we observed that the inhibitor influences the reservoir properties in a relatively small region around the well (approximately 3-4 meters). Nevertheless, the influence on the well pressure is remarkable. Indeed, for the reference case starting from 137 bars as initial value of the pressure at the well, during the normal production simulation this value decreases to 41 bars (70% loss) in 3522 days, while during the production with inhibitor simulation it decreases to 92 bars (32% loss). Higher values of the well pressure extend the well exploitation lifetime and decrease the operational cost of the process.

The sensitivity analysis shows that the injection time is a critical parameter in the design of the inhibitor injection treatment, while the inhibitor concentration appears to play a minor role. This could have relevant implications on the optimization of the treatment economical cost. The chemical affinity of the inhibitor with the reservoir rock has only a minor influence on the efficiency of the system, under the considered assumptions. Results of sensitivity analyses like the one we performed can assist practical investigations as they indicate which parameters should be further investigated to improve the control on the process.

Future developments. The model can be improved by including chemical equations for the precipitated species (for instance, calcite), which implies considering a) the modelling of the full geochemical system, b) the possibility of mineral dissolution. In the simplest case, still considering only one precipitating substance, the simplified aqueous system should be solved for the following unknown aqueous species:

$$H^+,\ OH^-, Ca^{2+}, CO_3^{2-}, HCO_3^-\ and\ H_2CO_3$$

Corresponding equilibrium reaction equations and mass action laws are presented as follows together with the equilibrium constants:

$$\begin{aligned} CO_2(g) + H_2O &= H_2CO_3 && K_h \\ H_2CO_3 &= H^+ + HCO_3^- && K_1 \\ HCO_3^- &= H^+ + CO_3^{2-} && K_2 \\ H_2O &= H^+ + OH^- && K_w \\ CaCO_3(s) &= Ca^{2+} + CO_3^{2-} && K_s \end{aligned}$$

$$[H_2CO_3] = K_1$$

$$\frac{[H^+][HCO_3^-]}{p} = K_1 K_h$$

$$\frac{[H^+][CO_3^{2-}]}{[HCO_3^-]} = K_2$$

$$[H^+][OH^-] = K_w$$

$$[Ca^{2+}][CO_3^{2-}] = K_s$$

Equilibrium constants are strongly dependent on the external factors such as pressure, pH and temperature, as documented in the literature. These parameters can be found in any geochemistry textbooks for standard temperature and pressure conditions, but the challenge appears when we need to consider large values of temperature and pressure.

The following future developments are envisaged at the end of this thesis work:

- perform additional simulations by fixing the pressure at the well-bottom instead of fixed flux, namely imposing the Dirichlet boundary condition at the well for the pressure;
- include multiple chemical species into the model or consider a multiphase flow which can be an improvement in the applicability of the model;
- couple the developed near-well model with a well-model, so that the fixed flux and/or the pressure at the well-bottom is not imposed but calculated through the well-model with the fixed flux/pressure at the well-head.
- extend the one-dimensional domain to two- or three-dimensional heterogeneous reservoir model which creates preferential channels and possibly changes the dynamics of nonlinear reactive processes such as the ones considered in this work.

APPENDIX

Well and reservoir data

- Well radius, r_w: 24 cm
- Drainage radius, R: 500 m
- Screen height, H: 5 m
- Initial average porosity, ϕ_0: 0.27
- Initial average horizontal permeability, k: 30 mD
- Production/Injection rate, Q : 100 m^3/day
- Initial well bottom-hole pressure, p_{w0}: 137 bars
- Reservoir temperature: 85 °C
- Average bulk density of reservoir, ρ_b: 2.5 kg/l
- Dispersivity, a_L: 0.12 m
- Rock type: Carbonate

Fluid properties

- Fluid density, ρ: 1 kg/l
- Fluid viscosity, μ: 1 cP
- Effective fluid compressibility, β: 10^{-8} kg/m^3/Pa^{-1}
- Equilibrium concentration of calcite: 0.03 mole/l
- Saturation index, Λ: 30
- Reaction constant, k_p: $1.1 \cdot 10^{-10}$ mole/m^2/s
- Specific surface area of the pore space, S: 10^3 m^3/m^2
- Molar volume of calcite, V_s : $36.93 \cdot 10^{-3}$ l/mole

Inhibitor properties:

- Recommended minimum inhibitor concentration: 10 mg/l
- Injected inhibitor concentration, c_{ifixed}: 35 g/l
- Maximum adsorption capacity, F_{max}: 1.280 mg/g
- Adsorption energy coefficient, b: 73 10^{-3} l/mg
- Inhibitor efficiency coefficient, η: 0.95
- Inhibitor efficiency exponent, n: 3

Characteristic values:

- $\hat{P} = 137$ bars
- $\hat{U} = 0.55$ m/hour
- $\hat{C} = 0.03$ mole/l
- $\hat{C}_\iota = 10$ mg/l
- $\hat{R} = 10$ m
- $\hat{K} = 30$ mD
- $\hat{T} = 30$ days

References

[1] F. Civan, Reservoir Formation Damage, Elsevier, 2015.

[2] J. W. Delleur, The handbook of groundwater engineering, CRC Press, 1999.

[3] J. Bear, Dynamics of Fluids in Porous Media, Dover, 2013.

[4] J. Bear and H.-D. Cheng, Modelling Groundwater Flow and Contaminant Transport, Springer, 2010.

[5] M. Wangen, Physical Principles of Sedimentary Basin Analysis, Cambridge University Press, 2010.

[6] R. J. Sterrett, Groundwater and wells, Johnson Screens, 2007.

[7] L. R. Jaworek, Calcium and Magnesium in groundwater, CRCPress, 2014.

[8] W. Stumm and J. Morgan, Aquatic Chemistry, John Wiley and Sons, 1996.

[9] CHIMEC, *Near-wellbore modelling of a scale inhibitor squeeze on a Libyan oilfield asset.*

[10] M. G. Lioliou, C. A. Paraskeva, P. G. Koutsoukos and A. C. Payatakes, "Calcium sulphate precipitation in the presence of water-soluble polymers," *Journal of Colloid and Int. Sci.,* 2006.

[11] A. Khormali, A. R. Sharifov and D. I. Torba, "Increasing efficiency of calcium sulphate scale prevention using a new mixture of phosphonate scale inhibitors during water flooding," *Journal of Petr. Sci. and Eng.,* 2018.

[12] Z. Chen, G. Huan and Y. Ma, Computational Methods for Multiphase Flows in Porous Media, Philadelphia: SIAM, 2006.

[13] I. Borsi and A. Fasano, "A general model for bioremediation processes of contaminated soils," *Int. J. Adv. Eng. Sc. Appl. Math.,* 2009.

[14] I. Borsi, A. Farina, A. Fasano and M. Primicerio, "Modelling bioremediation of polluted soils in unsaturated condition and its effect on the soil hydraulic properties," *Appl. Math.,* 2008.

[15] M. Wangen, J. Sagen, T. Bjornstad, H. Johansen and A. Souche, "Models for Calcium Carbonate Precipitationin the Near-Well Zone by Degassing of CO2," *The Open Petr. Eng. Journal,* 2016.

[16] "PHREEQS Documentation," [Online]. Available: https://pubs.usgs.gov/tm/06/a43/pdf/tm6-A43.pdf.

[17] E. Stamatakis, A. Stubos and J. Muller, “Scale prediction in liquid flow through porous media: A geochemical model for the simulation of CaCO3 deposition at the near-well region,” *Journal of Geochemical Exp.,* 2010.

[18] Y. Zang and R. Dawe, “The kinetics of calcite precipitation from a high salinity water,” *Applied Geochemistry,* 1997.

[19] H. Sundqvist and G. Veronis, “A simple finite-difference grid with non-constant intervals,” 1970.

[20] A. Quarteroni, Numerical Models for Differential Problems, Springer-Verlag, 2014.

[21] T. M. A. K. Azad and L. S. Andallah, “Stability Analysis of Finite Difference Schemes for an Advection Diffusion Equation,” *Bang. J. Sci. Res.,* 2016.

[22] M. Thongmoon and R. McKibbin, “A Comparison of Some Numerical Methods for the Advection-Diffusion Equation,” *Res. Lett. Inf. Math. Sci.,* 2006.

[23] I. B. Celik, U. Ghia, P. J. Roache, C. J. Freitas, H. Coleman and P. E. Raad, “Procedure for estimation and reporting of uncertainty due to discretization in CFD applications,” *Journal of fluids {Engineering-Transactions} of the {ASME},* 2008.

[24] P. J. Roache, “Quantification of Uncertainty in Computational Fluid Dynamics,” *Annu. Rev. Fluid. Mech.,* 1997.

[25] G. Porta, D. la Cecilia, A. Guadagnini and F. Maggi, “Implications of uncertain bioreactive parameters on a complex reaction network of atrazine biodegradation in soil,” *Advances in Water Res.,* 2018.

[26] S. Naseri, J. Moghadasi and M. Jamialahmadi, “Effect of temperature and calcium ion concentration on permeability reduction due to composite barium and calcium sulphate precipitation in porous media,” *Journal of Natural Gas Sci. and Eng.,* 2014.

[27] “FiPy: A Finite Volume PDE Solver Using Python, Version 3.1.2,” [Online]. Available: http://www.ctcms.nist.gov/fipy/documentation/contents.html.

[28] A. Hernandez, A. La Rocca, H. Power, U. Graupner and G. Ziegenbalg, “Modelling the effect of precipitation inhibitors on the crystallization process from well mixed over-saturated solutions in gypsum based on Langmuir-Volmer correction,” *Journal of Crystal Growth,* 2006.

[29] F. Yan, F. Zhang, N. Bhandari, L. Wang, Z. Dai, Y. Liu, G. Ruan, A. Kan and M. Tomson, “Adsorption and precipitation of scale inhibitors on shale formations,” *Journal of Petr. Sci. and Eng.,* 2015.

[30] A. Satman, Z. Ugur and M. Onur, “The effect of calcite deposition on geothermal well inflow performance,” *Geothermics,* 1999.